iScience

CellPress
OPEN ACCESS

Article

Atypical cadherin, Fat2, regulates axon terminal organization in the developing *Drosophila* olfactory receptor neurons

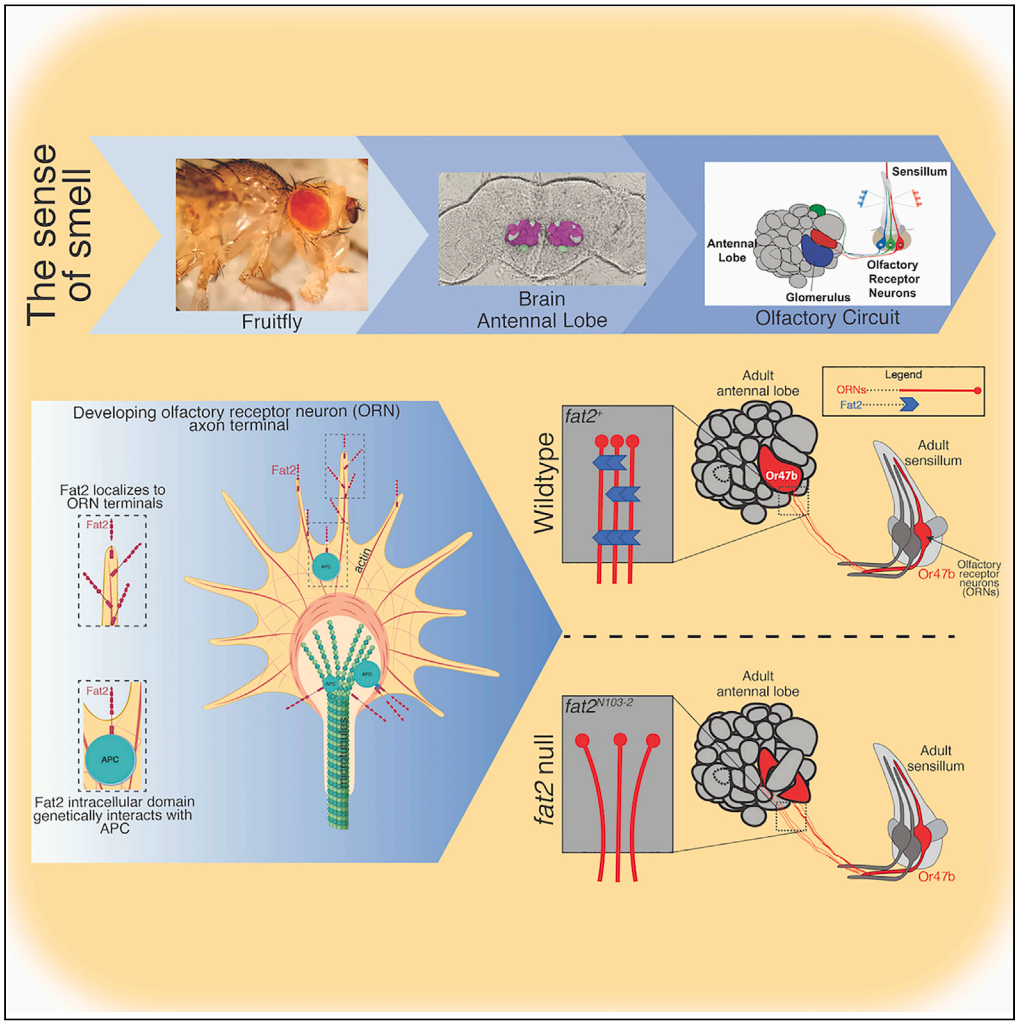

Khanh M. Vien, Qichen Duan, Chun Yeung, Scott Barish, Pelin Cayirlioglu Volkan

pelin.volkan@duke.edu

Highlights

ORN expression of Fat2-ICD is necessary for class-specific glomerular organization

Fat2-ICD genetically interacts with APC for appropriate glomerular morphology

Fat2 shows differential expression and functional requirement across ORN classes

Vien et al., iScience *27*, 110340
July 19, 2024 © 2024 The Author(s). Published by Elsevier Inc.
https://doi.org/10.1016/j.isci.2024.110340

iScience

CellPress
OPEN ACCESS

Article

Atypical cadherin, Fat2, regulates axon terminal organization in the developing *Drosophila* olfactory receptor neurons

Khanh M. Vien,[1] Qichen Duan,[1] Chun Yeung,[1] Scott Barish,[1,3] and Pelin Cayirlioglu Volkan[1,2,4,*]

SUMMARY

The process of how neuronal identity confers circuit organization is intricately related to the mechanisms underlying neurodegeneration and neuropathologies. Modeling this process, the olfactory circuit builds a functionally organized topographic map, which requires widely dispersed neurons with the same identity to converge their axons into one a class-specific neuropil, a glomerulus. In this article, we identified Fat2 (also known as Kugelei) as a regulator of class-specific axon organization. In *fat2* mutants, axons belonging to the highest *fat2*-expressing classes present with a more severe phenotype compared to axons belonging to low *fat2*-expressing classes. In extreme cases, mutations lead to neural degeneration. Lastly, we found that Fat2 intracellular domain interactors, APC1/2 (Adenomatous polyposis coli) and *dop* (Drop out), likely orchestrate the cytoskeletal remodeling required for axon condensation. Altogether, we provide a potential mechanism for how cell surface proteins' regulation of cytoskeletal remodeling necessitates identity specific circuit organization.

INTRODUCTION

In both insects and mammals, odor detection relies upon the topographic map created by diverse classes of olfactory neurons that organize their axons to converge in a class-specific manner within the antennal lobe in flies, or the mammalian central brain's olfactory bulb.[1,2] Given its intricate association with neurodegeneration and neuronal dysfunction, decoding the mechanisms underlying how diverse classes of neurons organize their axons represents a significant pursuit in the field of neurobiology. In flies, olfactory receptor neuron (ORN) classes are defined by the selective co-expression of generally one to three odorant receptor (and/or ionotropic receptor) combinations.[3] ORNs belonging to the same class (one of the around fifty possible classes) converge their axons to a single neuropil, called a glomerulus, and synapse with second-order projection neurons (PNs). This organizational logic is known colloquially as the "one olfactory receptor, one glomerulus" rule. Considering the stereotyped shapes, boundaries, and positionings of the glomerular map, each ORN class likely has a unique set of instructions that is shared across neurons belonging to that class. Previously, we and others have shown that the disruption of several cell surface molecules, such as Cadherin family proteins, can disrupt class-specific glomerular organization.[4,5] Leveraging the field's detailed understanding of the Drosophila olfactory circuit architecture and development, we can reveal these cell surface molecules' mechanisms of action responsible for the regulation of large-scale tissue organization.

The adult Drosophila olfactory system is an excellent model for studying neurodevelopment because it utilizes biological processes documented across most developing multi-cellular neural networks, such as direct the behaviors of neuronal processes via the temporal and spatial regulation of various cell surface molecules. During metamorphosis, adult ORNs are born within the eye-antennal imaginal disc and all ~1200 ORNs per antenna must extend their axons great distances into the central brain.[6] Around 16–18 hAPF (hours after pupal formation) ORN axons reach the antennal lobe[7] and begin to snake along the antennal lobe surface with transient exploratory branches surveying the environment for their target glomerulus.[8] Between 20 hAPF and 40 hAPF, the exploratory axons target a glomerulus,[9,10] interact with PNs and local interneurons (LNs),[11,12] and then begin to simultaneously repel from adjacent glomeruli while converging with class-specific axons to further accentuate proto-glomerular boundaries.[4,13] The mechanisms critical to the stabilization of these transient axonal branches are unknown, and likely involve proteins that link chemoaffinity receptor activity to cytoskeletal regulators. The litany of cell surface proteins implicated in olfactory system development, such as Semaphorins, DSCAM, Tenascins/Teneurins and Toll receptors, suggests that ORN class-specific cell surface codes are the main drivers of this topographic circuit assembly.[9,11,13–18] Though there are several examples of cell surface molecules regulating ORN class-specific axon organization, it is still unclear when and how ORN class-specific axon convergence occurs during olfactory circuit development.[4,15,16,19]

[1]Department of Biology, Duke University, Durham, NC 27708, USA
[2]Department of Neurobiology, Duke University Medical Center, Durham, NC 27710, USA
[3]Present address: Colossal Biosciences, Dallas, TX 75247, USA
[4]Lead contact
*Correspondence: pelin.volkan@duke.edu
https://doi.org/10.1016/j.isci.2024.110340

This is an open access article under the CC BY-NC-ND license (http://creativecommons.org/licenses/by-nc-nd/4.0/).

Given the importance of cell surface combinatorial codes, identifying novel cell surface proteins functionally required for olfactory circuit assembly is critical to decrypting the "rosetta stone" needed to translate cell surface signatures into predictable discrete cellular processes. Given the close association between the evolution of Cadherin family proteins and the emergence of the synapse,[20] it is unsurprising that members of the Cadherin family (N-cadherin and protocadherins) have been shown to regulate aspects of neuronal organization,[21] and specifically insect and mammalian olfactory circuit development.[4,22] While highly expressed in the developing olfactory circuit and considered most closely related to the common ancestor of modern cadherins,[23] Fat cadherins and their role in neuronal organization have not been investigated in the developing olfactory system. Fat cadherins, the largest members in the Cadherin family, have 34–36 cadherin repeats in their extracellular domain,[4,24] which is more than twice the length of Drosophila N-Cadherin, a well-known organizer of protoglomerular organization, which has 17 cadherin repeats. Due to the size of Fat2, a major obstacle to studying the *in vivo* function of this protein is the difficult and cumbersome molecular biology required to generate functional genetic tools. Recent generation of whole animal null mutants, domain-specific mutants, and GFP-tagged Fat2 direct fusion protein, allows us to functionally characterize this highly conserved protein in a neuronal context.[25–27]

Fat cadherins are an appealing target due to their remarkable sequence conservation and their highly specific expression in the developing olfactory centers across the animal kingdom.[28,29] Notably, it has been proposed that the contemporary protocadherin ectodomains may have arisen from the gradual reduction of N-terminal cadherin domains in the ancestral Fat protein, further underscoring the significance of studying these proteins.[23] Compared to the four Fat cadherins in mammals, Drosophila has two Fat cadherins, Fat and Fat2 (also known as Kugelei, or Fat-like cadherin), which share striking homology to Fat4 and Fat1/3 in humans, respectively.[29] It is important to note that the intracellular domains of Drosophila Fat and Fat2 exhibit substantial divergence, characterized by distinct sets of interacting partners that do not overlap. These findings strongly indicate that these two proteins serve distinct functional roles in biological processes. Fat2, and its vertebrate orthologues Fat1 and Fat3, has been shown, using RNA-seq, qRT-PCR, and *in situ* hybridization, to be most highly expressed within the developing olfactory bulb and has been associated with several human neuropathologies.[30–32] The role of Fat2 has been revealed in several mammalian sensory circuits (such as retinal development and cochlear morphogenesis) and Drosophila tissue morphogenesis, yet the function of Fat2 in olfactory circuit development is unknown.[26,27,33,34] Here we demonstrate that the Drosophila Fat2 protein organizes glomerular architecture by promoting class-specific ORN axon bundle convergence. In *fat2* mutants, we observed that many ORN classes displayed fragmented glomeruli with varying severity. By utilizing intersectional genetic approaches, we have identified that Fat2 expression varies across ORN classes during mid-pupal development and is expressed by a unique subpopulation of antennal lobe local interneurons. We have further characterized Fat2 protein localization to axon terminals and provided evidence that the intracellular signaling domain is necessary for its function in glomerular organization. Finally, we present evidence suggesting that Fat2 regulates axon behavior by interacting with cytoskeletal remodeling proteins.

RESULTS

Genetic disruptions of Fat2 result in abnormal glomerular organization

Fat3 and Fat1, mammalian orthologues of Drosophila Fat2, are documented to be specifically and highly expressed in the olfactory bulbs of developing rats and mice.[31,35,36] Consistent with the expression data, several studies in mice show disruptions in Fat3/Fat1 result in a faulty neural organization, in both auditory and visual sensory systems.[37,38] In order to derive the direct impact of Fat2 disruptions on fly olfactory circuit organization, we restrictively knocked down *fat2* expression using the ORN-specific driver *pebbled-GAL4* (*peb-GAL4*) to drive *fat2* RNAi. To assess the effect of *fat2* knockdown on class-specific glomerular architecture, we visualized one of the largest and most easily identifiable glomeruli innervated by Or47b ORNs using *Or47b-CD2*. We found that compared to *peb-GAL4* only controls (13% aberrant glomerular morphology, $n = 52$) or *UAS-fat2 RNAi* only controls (10%, $n = 54$), experimental brains (37%, $n = 60$) resulted in Or47b ORNs-innervated VA1v glomerulus becoming morphologically deformed, including glomerular rotation, shape change, and/or fragmentation (Figure 1B; Figure S1). While the parallels between Fat2 and its mammalian counterparts, Fat3 and Fat1, have been implicated in neural circuit development, our study offers direct insights into the consequences of Fat2 disruption in the olfactory system.

We set out to investigate whether the role Fat2 plays on ORN neuropil organization can also be applied to other glomeruli. To test this, and corroborate our RNAi knockdown results, we visualized four glomeruli (Or47a, Or23a, Or47b, and Gr21a) in whole animal mutants with various *fat2* null alleles. With this paradigm, we were able to compare the morphology of each glomerulus in control brains (11%, $n = 17$), homozygous Fat2 null mutant ($fat2^{N103\text{-}2}$) (77%, $n = 26$), and *trans*-heterozygous mutant for two separately generated *fat2* null alleles ($fat2^{N103\text{-}2}/fat2^{58D}$) (37%, $n = 32$) (Figures 1D–1G; Figure S1). $fat2^{N103\text{-}2}$ is a null allele containing a premature stop codon at position 3718,[25] and $fat2^{58D}$ is a null allele that contains a deletion for the amino acids 1–687 including the start codon.[39] In these whole animal mutants, we observed three glomeruli targeted by Or47a, Or23a, and Or47b ORNs exhibit organizational disruptions. Supporting our previous data, we found that whole animal mutants phenocopy ORN-specific *fat2* RNAi knockdown animals in VA1v glomerulus (Figures 1B′, 1D″, and 1F′). We found a variety of morphological disruptions to each of the three glomeruli (Figure S2). For clarity, we have designated disruptions to any glomeruli as a "disrupted" brain and included the more detailed quantification in the supplementals (Figure S1). We interpreted the presence of ectopic glomeruli and ectopic axon projection as possibly a result of a loss of class-specific axon aggregation. Heterozygous Fat2 null mutants did not exhibit any glomerular disruptions (Figure 1D′).

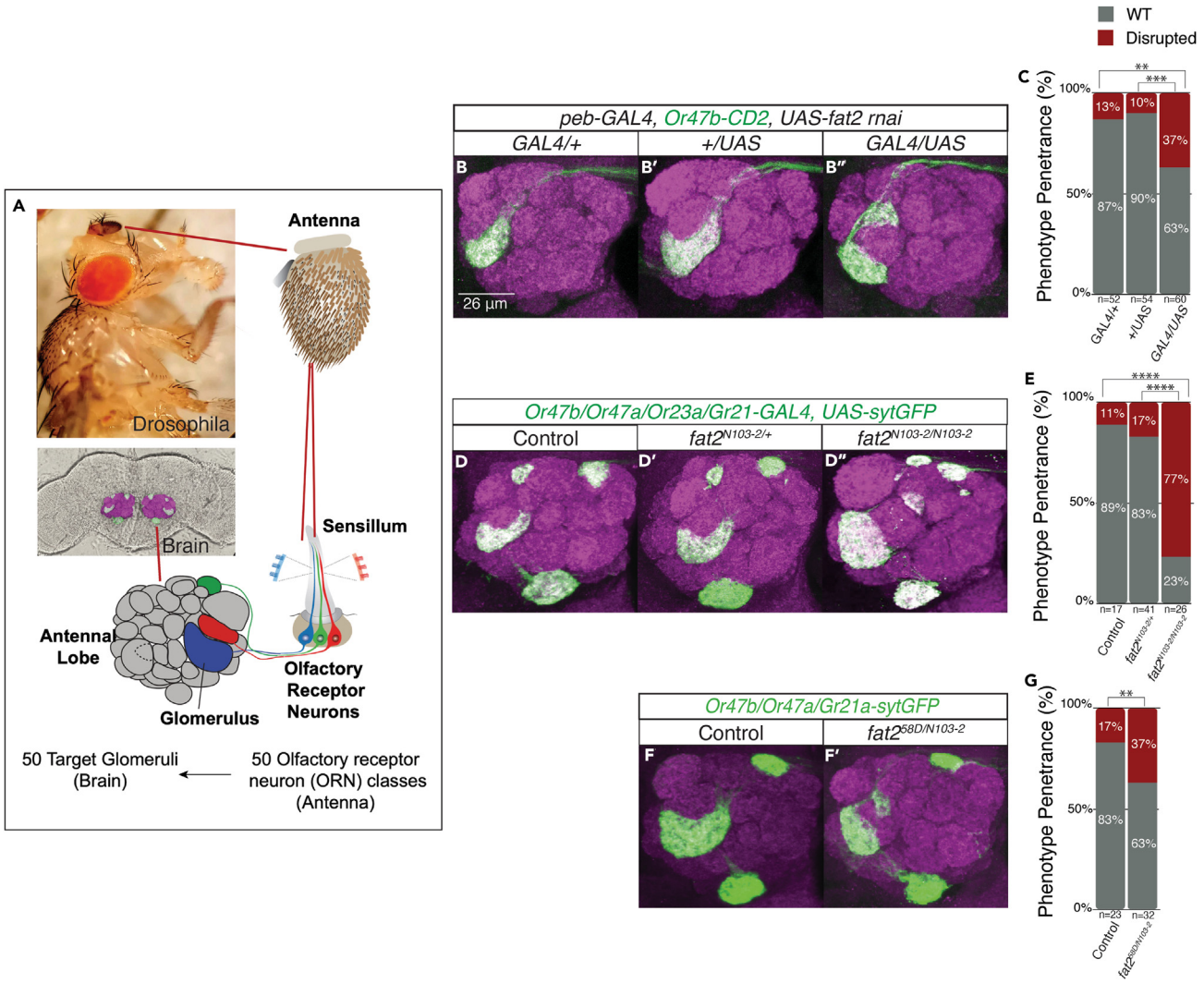

Figure 1. Genetic disruptions in *fat2* breaks stereotype olfactory glomeruli morphology

(A) Schematic to illustrate the neural architecture of the drosophila olfactory system.

(B-B′′) Representative z stack images of the glomeruli (VA1v) innervated by Or47b axon terminals (green) co-stained with antibody against N-Cadherin (magenta) to visualize antenna lobe structure. Pan-ORN (*peb-GAL4*) RNAi knockdown of *fat2* results in a split VA1v glomerulus.

(C) Quantification of brains with disrupted glomerular morphology for experiment in (B). (No *GAL4*) Control (n = 52) and (No *UAS*) Control (n = 54) are not significantly different. Both controls compared to *peb>fat2 RNAi* (n = 60) using Fisher's exact test (**p = 0.0027, ***p = 0.0004).

(D-D′′) Representative z stack images of glomeruli innervated by Or47b, Or47a, Or23a, and Gr21a axon terminals (green) co-stained with anti-N-Cadherin (magenta) in Control (D), heterozygotes for *fat2* null (*fat2*$^{N103-2}$) (D′), and homozygous *fat2* null whole animal mutants (D′′). *Or47b-*, *Or47a-*, *Or23a-*, and *Gr21a-GAL4, UAS-sytGFP* transgenic flies were used. Homozygous *fat2* null whole animal mutants break apart the continuous neuropil for Or47b, Or47a, and Or23a ORNs.

(E) Quantification of brains with disrupted glomerular morphology for Control (n = 34), heterozygous for *fat2* null (*fat2*$^{N103-2}$) (n = 41), and homozygous for *fat2* null (n = 26) using Fisher's exact results in ****p <0.0001.

(F) *Trans*-heterozygote of two different *fat2* null alleles from separate labs phenocopy homozygous *fat2*$^{N103-2}$ mutant phenotype. *Or47b*, *Or47a*, *Gr21a* visualized via direct fusion to *sytGFP* and then stained with the same antibodies as (B).

(G) Using Fisher's exact test to compare Control (n = 23), and *fat2*$^{N103-2}$/*fat2*^{58D}(n = 32) results in significance of **p = 0.0011. Scale bar shows 26 µm.

See also Figures S1, S2, and S11.

To summarize, both ORN-specific RNAi knockdown of *fat2*, as well as whole animal mutants for homozygous and transallelic *fat2* null alleles result in disruptions to the organization of multiple glomeruli across the antenna lobe. Consistent with our finding, a previous study also reported that pan-neuronal knockdown of *fat2* resulted in a disrupted Drosophila olfactory circuit architecture.[40] The observed deformations in the olfactory circuitry emphasize the significance of Fat2 in maintaining the integrity of class-specific glomerular architecture.

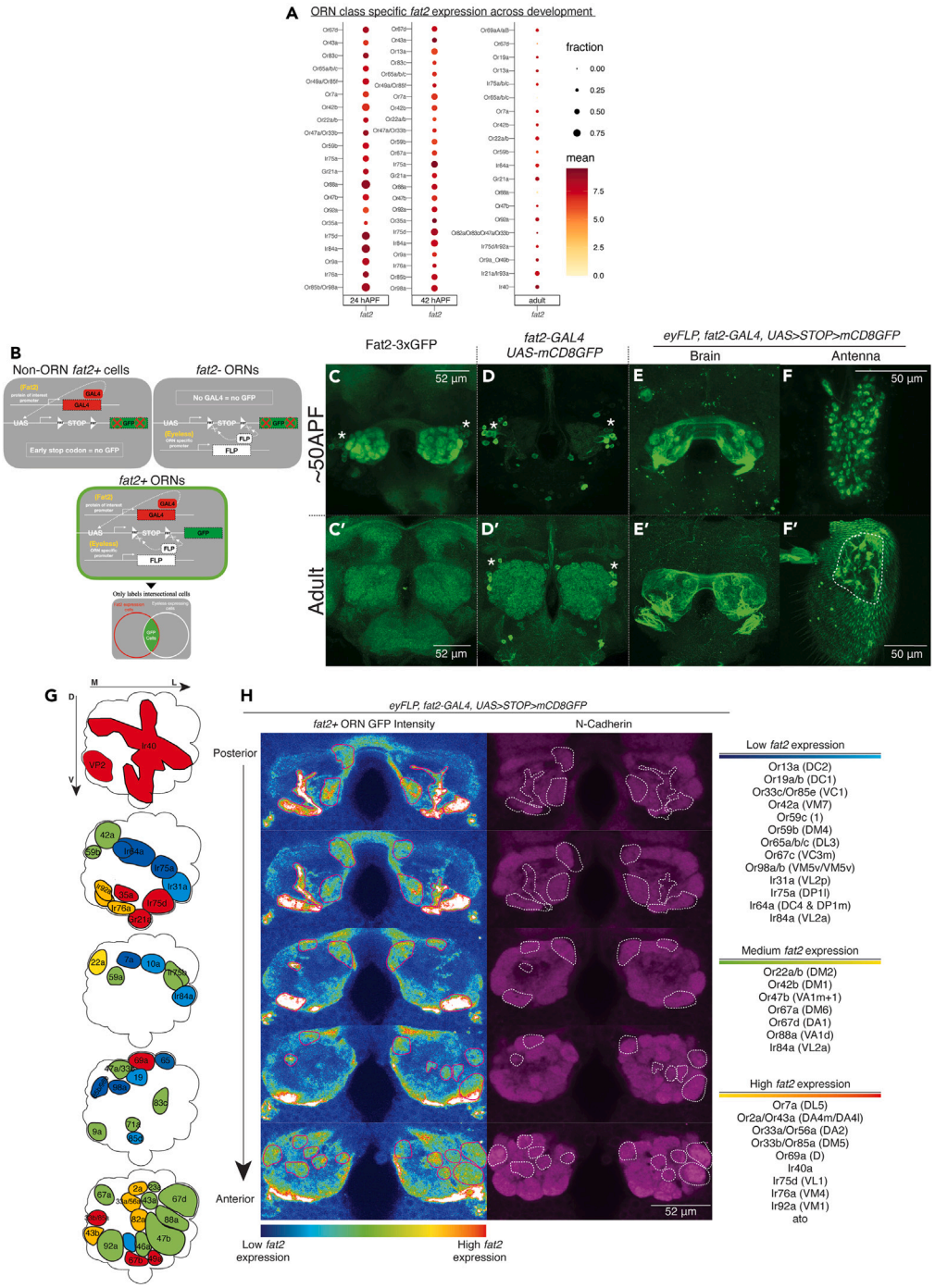

Figure 2. Pupal olfactory system shows developmentally distinct *fat2* expression and Fat2 protein sub-cellular localization

(A) Dot plot summary of *fat2* expression per select ORN class at 24 hAPF, 48 hAPF, and adult using previously published single-cell RNA-seq datasets.

(B) Visual representation of the genetic tools and logic used to orchestrate the intersectional labeling of *fat2*-positive ORNs.

(C–F, C′–F′) 50 hAPF pupal brains and adult brains stained with anti-GFP for Fat2-3xGFP (fat2 directly fused to GFP), *fat2-GAL4* driven *UAS-mCD8GFP*, and intersectional labeling of *fat2*-positive ORNs using *eyFLP, fat2-GAL4, UAS>STOP>mCD8GFP*. Antennal images also stained with anti-GFP for *eyFLP, fat2-GAL4, UAS>STOP>mCD8GFP* to visualize *fat2*-positive ORN cell bodies. Cell bodies of unknown identity adjacent to the antenna lobe are also positive for *fat2* expression, marked with white asterisks.

(G) Cartoon representation of stereotypical glomerular positioning within the antennal lobes. Color of glomerulus represents the qualitative *fat2* expression level.

Figure 2. *Continued*

(H) *eyFLP, fat2-GAL4, UAS>STOP>mCD8GFP* pupa at 70 hAPF. Heatmap representing GFP fluorescence intensity and N-Cadherin antibody stain in magenta to identify glomeruli position. Stereotypical location and shape of each glomerulus are visually assessed and assigned an ORN class based on olfactory maps described in the literature.[1,3,41] Scale bar shows 50 or 52 μm.

See also Figures S3–S6.

Fat2 expression changes throughout olfactory system development

One possible mechanism by which Fat2 regulates glomerular organization is by establishing an expression level signature unique to each ORN class. To get a brief idea of which ORN class(es) express Fat2, we analyzed published single-cell RNA-seq data to produce a list of Fat2-expressing ORN classes (Figure 2A).[32] Based on our analysis, Fat2 seems to be broadly expressed across ORN classes (Figure 2A). Consistent with its role in olfactory system development, Fat2 exhibits higher expression levels at 24 hAPF and 48 hAPF compared to its expression level in adult ORNs. This expression profile aligns with our earlier findings, further substantiating the notion that Fat2 plays a pivotal role in shaping class-specific synaptic neuropils during the development of the olfactory circuit.

Unfortunately, this antennal single-cell RNA-seq dataset captures only a limited portion of all ORN classes. Therefore, to uncover a more complete *fat2* expression profile, we utilize two genetic approaches: an intersectional genetic approach and GFP-tagged Fat2 recombinant protein analysis. To perform the intersectional labeling of *fat2*-positive ORNs, we enlist the ORN-specific *eyeless* promoter to drive flippase expression (*ey-FLP*), the *fat2* promoter-driven expression of GAL4 (*fat2-GAL4*), and membrane-bound GFP silenced with an upstream FRT-flanked stop cassette *(UAS>STOP>mCD8GFP*). The combination of these three genetic tools allows us to restrict GFP fluorescence signal to only cells that express both *eyeless* and *fat2* (Figure 2B). Flippase (FLP)-directed excision of the FRT-flanked stop cassette is required to allow GAL4 (expressed in *fat2*-positive cells) to drive the expression of GFP. Therefore, only cells with both FLP and GAL4 can drive the expression of mCD8GFP, effectively labeling only *fat2*-positive ORNs. We analyzed the GFP expression pattern during various points of olfactory system development to visualize the developmental dynamics and heterogeneity of *fat2* expression across ORN populations (Figures 2E–2H; Figures S3, S4, and S6). We found that Fat2 is not expressed by ORNs until after 24 hAPF (Figure S3)**.** Fat2 expression within the antennal lobe begins between 30 and 40 hAPF. The difference in fluorescence intensity within the antennal lobes between *fat2-GAL4 UAS-mCD8GFP* and Fat2-3xGFP is due to the lower camera exposure used in *fat2-GAL4 UAS-mCD8GFP* brains in our attempt to not oversaturate the cell bodies adjacent to the AL (Figures 2C and 2D). Due to this reason, when the cell bodies adjacent to the antennal lobe are absent (such as in our intersectional labeled brain) the exposure is returned to a higher level conducive to seeing the lower fluorescence within the antennal lobe (Figure 2E). We noticed variable levels of green fluorescence across glomeruli suggesting differential *fat2* expression levels across ORN classes (Figures 2E and 2H; Figures S3 and S5). To quantitatively confirm the differential fluorescence levels between ORN classes, we measured the mean fluorescence intensity of select glomeruli (we selected ORN classes that were both representative of the three fat2 expression tiers and were also identifiable in developing pupal brains) across four different brains and were indeed able to measure significant fluorescence intensity differences across ORN-classes (Figure S2). In adults, we found that ORNs belonging to Ir40a, Ir75d, and Ir76b classes and their respective glomeruli showed the highest levels of Fat2 expression[41] (Figure 2H). Our results corroborate the list of *fat2*-expressing ORN classes generated from the single-cell RNA-seq data (Figure 2A). Even though inter-glomerular fluorescence signal variation seems to be maintained throughout pupal development, overall antennal lobe fluorescence is highest between 42 hAPF and 48 hAPF (Figure S1). Aside from glomeruli targeted by Ir (ionotropic receptor)-expressing ORNs, *fat2* expression was also higher in glomeruli targeted by Or19a, Or13a, and Or56a ORNs (Figure S3). The lowest levels of *fat2* expression were observed for glomeruli targeted by Ir64a and Ir84a ORNs. To confirm that the glomerular fluorescence signal is coming from ORN projections and not from other antennal lobe neurons, we analyzed the GFP fluorescence in the antennae, where ORN cell bodies reside (Figures 2F and 2F′). We found an abundance of *fat2*-positive ORN cell bodies throughout the mid-pupal antennae (Figure 2F), suggesting that the majority of ORNs express Fat2 during pupal development. Yet as the fly matures, high Fat2 expression becomes restricted to ORN cell bodies originating from the sacculus in the adults (Figure 2F′). Two key observations emerged: firstly, fat2 expression displays inter-glomerular variability, hinting at a potential ORN class-specific expression pattern, while showing no discernible variation within individual glomeruli. Secondly, the initiation of fat2 expression at approximately 30 hAPF coincides with the onset of protoglomerular formation, suggesting its integral role in this crucial developmental process.

If Fat2 is expressed in ORNs to regulate the class-specific organization of axons and axon terminals, we would predict Fat2 to localize along ORN axons and synapses as opposed to ORN cell bodies. To probe Fat2 protein sub-cellular localization, we leveraged a CRISPR-generated transgenic Drosophila line with three copies of GFP tagged to the C-terminus of Fat2 (Fat2-3xGFP).[27] Within the brain, we found that GFP fluorescence intensity was higher during pupal stages compared to that in adults (Figures 2C and 2C′), which is consistent with data from single-cell RNA-seq and *fat2-GAL4* expression patterns (Figures 2D and 2D′). Further supporting the functional role of Fat2 in organizing ORN axons, we found that Fat2-3xGFP fluorescence was predominantly confined to the antennal lobe and commissural tract, which indicates localization along ORN axon projections and terminals (Figure 2C). On the other hand, we did not see any fluorescence in either pupal or adult ORN cell bodies on the antennae (Figure S5), suggesting that Fat2 protein is indeed primarily trafficked to neuronal projections during development.

In summary, our results indicate that Fat2 is localized to ORN axons and projection terminals within the neuropils. Furthermore, Fat2 displays specificity in its expression levels within individual class-specific glomeruli and undergoes changes in expression throughout development. The insight gained from the expression data implicates Fat2 specifically in the mid-pupal protoglomerular development.

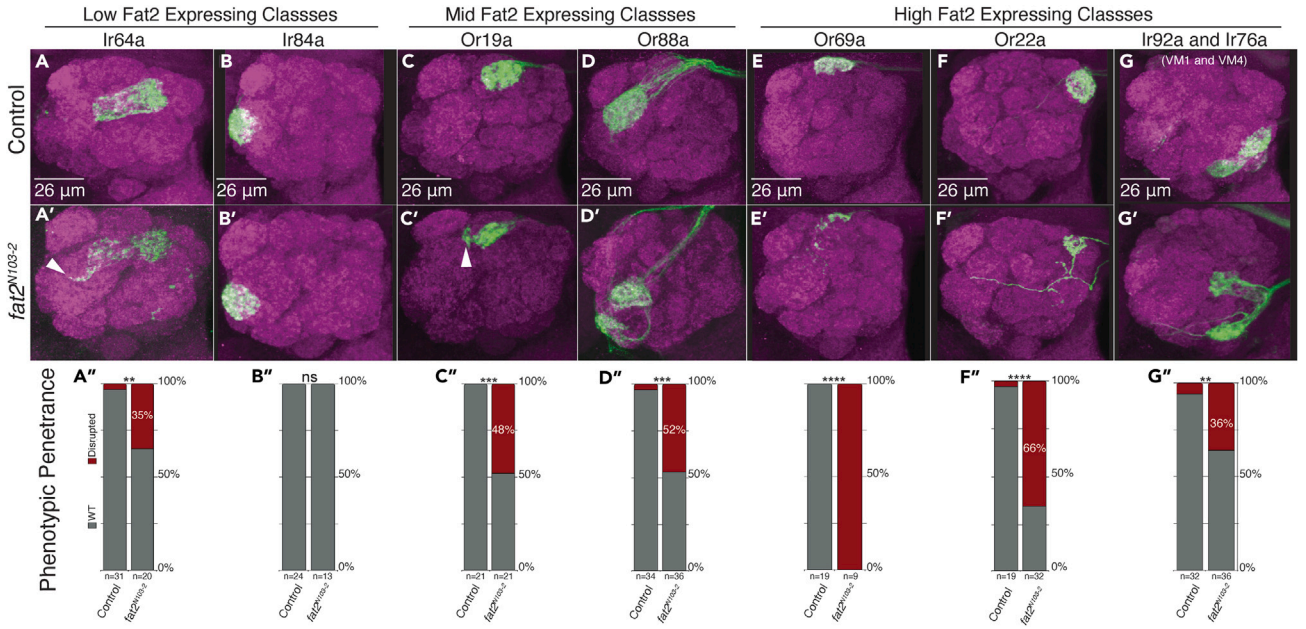

Figure 3. Class-specific *fat2* expression levels predict severity of *fat2* null mutant phenotypes

(A–G, A′–G′) Representative z stack composite images of single antenna lobes visualizing two low *fat2* expressing ORN classes (Ir64a and Ir84a), two mid *fat2* expressing classes (Or19a and Or88a), and three high *fat2* expressing classes (Or69a, Or22a, Ir92a, and Ir76a). Control and $fat2^{N103\text{-}2}$ homozygotes are stained with anti-GFP (green) to show axon terminals and anti-N-Cadherin (magenta) for antennal lobe gross anatomy. Each ORN class is labeled using *OrX-GAL4* (or *72OK-GAL4* for Ir92a and Ir76a) and *UAS-sytGFP*. Aberrations in glomerular structure (emphasized with white arrows) seen in mutant alleles but rarely, if ever, appear in control brains. (A″–G″) Bar graphs quantifying phenotypic penetrance in Control (A-G) and *fat2* null homozygotes (A′–G′). Fisher's exact test performed on quantifications (A″) 35% disrupted phenotype in $fat2^{N103\text{-}2}$ mutants, $p = 0.004$; (B″) 0%, not significant; (C″) 48%, $p = 0.0005$; (D″) 52%, $p < 0.0001$; (E″) 100%, $p < 0.0001$; (F″) 66%, $p < 0.0001$; (G″) 36%, $p = 0.007$. Scale bar shows 26 µm.

See also Figures S2, S7, and S11.

Fat2 expression level parallels class-specific glomerular phenotypes in *fat2* mutants

We then set out to test how the differential expression levels of *fat2* across ORN populations contribute to the class-specific glomerular organization. Using the results from the intersectional labeling approach and the known glomerular map, we were able to identify and categorize ORN classes into high and low *fat2* expressing classes (Figure 2H).[1,3,42] Then using this list and the available transgenic tools to label each ORN class, we analyzed the glomerular organization in wild type and *fat2* null ($fat2^{N103\text{-}2}$) whole animal mutants. To determine the effect of *fat2* mutations on ORN classes expressing high levels of Fat2, we analyzed D, DM2, VM4, and VM1 glomerular morphology targeted by Or69a (100% disrupted phenotype, $n = 9$), Or22a (66%, $n = 32$), Ir76a and Ir92a (36%, $n = 36$) ORNs (Figures 3E–3G). For classes that express medium levels of Fat2, we analyzed DC1 and VA1d glomeruli innervated by Or19a (48%, $n = 21$) and Or88a (52%, $n = 36$) ORNs (Figures 3C and 3D). And lastly to assess glomeruli expressing low levels of Fat2, we analyzed DC4/DP1m and VL2a glomerular morphology targeted by Ir64a (35%, $n = 21$) and Ir84a (0%, $n = 13$) ORNs (Figures 3A and 3B′). The most common morphological perturbation we found across ORN classes that show a phenotype is the fragmentation or discontinuity of what should be a single glomerulus. The glomerular phenotypes observed in fat2 null mutants differ among Or-classes, with Ir64a displaying minimal to no fragmentation (only 5% has ectopic projection, 1/20 brains; the other disrupted brains had glomerular extensions) in its glomerular field. Conversely, the intermediate and high-expressing classes exhibit the clear fragmentation of their glomerular fields (Figure S2). This variance in the extent of fragmentation leads us to infer that Ir64a may be less susceptible to the effects of *fat2* disruption. Considering this difference in response to *fat2* disruption, we note a trend where higher-expressing classes tend to display increased fragmentation and a higher proportion of disrupted brains. In addition to disruptions in glomerular morphology, we found that glomerulus D innervated by Or69a ORNs completely disappeared in *fat2* mutants. This is likely due to decreasing ORN cell number since seven+-day-old flies homozygous for *fat2* null alleles exhibit antennal degeneration (Figure S7). The variation in glomerular phenotypes suggests that ORN classes show differential requirements for Fat2 function, likely based on expression levels.

In summary, likely due to ORN class-specific differences in the level of Fat2 expression, we observed variable penetrance and expressivity of the glomerular disruption phenotypes across ORN classes analyzed. This suggests that the Fat2-dependent regulation of axon organization is Or-class specific. Additionally, we noticed Or69a ORNs, which are among the ORN classes with the highest levels of *fat2* expression, experience the highest percentage of disrupted brains in response to loss of *fat2* function. Meanwhile, Ir84a ORNs, which are among the classes with the lowest levels of *fat2*, appears wild type in *fat2* mutants.

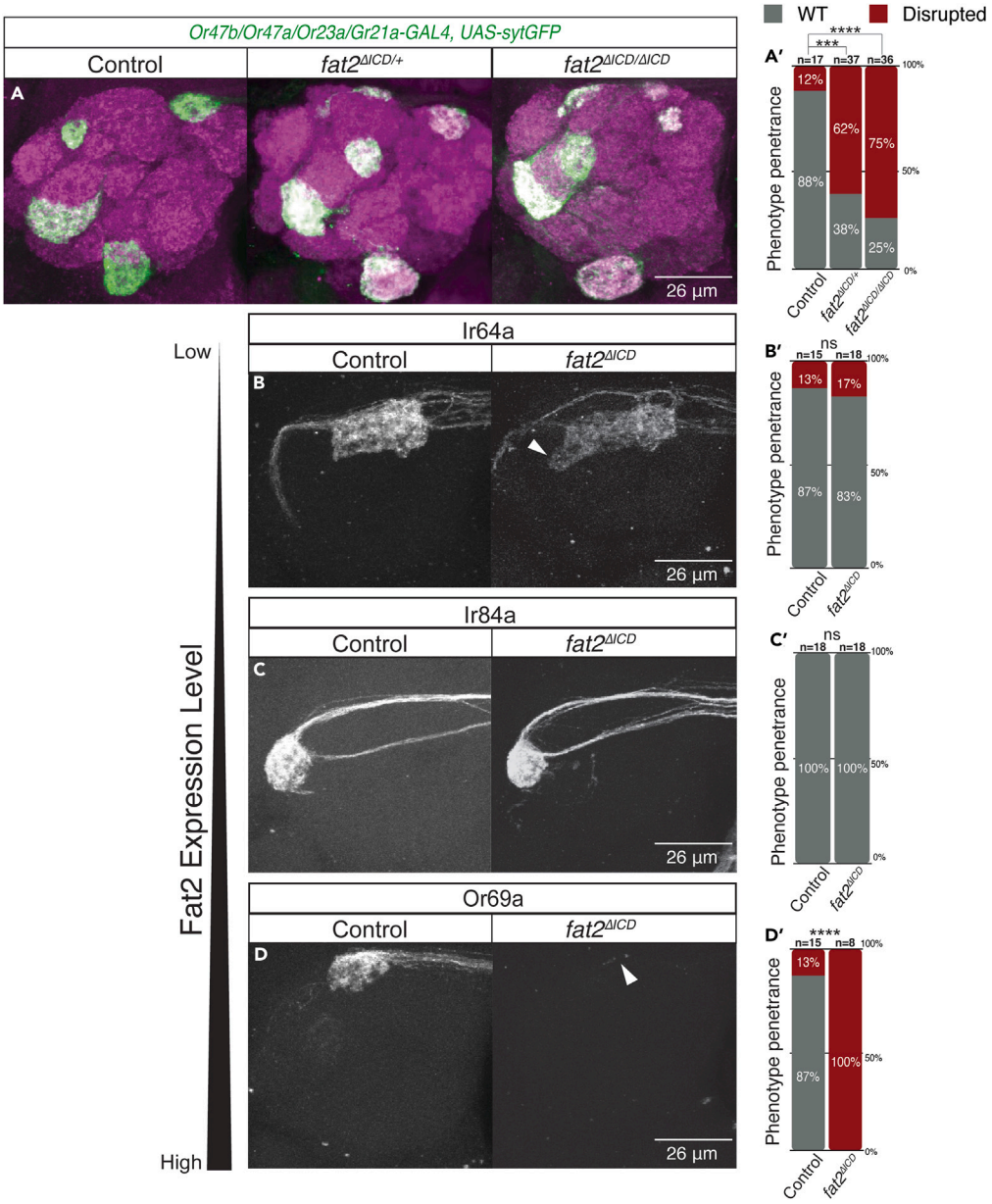

Figure 4. Fat2 intracellular domain mutant, with intact extracellular domain, phenocopies *fat2* null mutant glomerular phenotype in a class-specific manner

(A–D) Representative z stack composite images of single antenna lobes. Only panel (A) is stained with anti-GFP and anti-N-Cadherin. All other images were unstained. In(B-D) each ORN class is labeled using the same *OrX-GAL4* as Figure 3 but instead drives the expression of *10xUAS-RFP*. $fat2^{\Delta ICD}$ brains were from flies homozygous for the $fat2^{\Delta ICD}$ allele.

(A′–D′) Bar graph quantification of brains with glomerular disruptions (red bar). Fisher exact test for (A′) and (D′), separately, resulted in ****p <0 .0001 and ***p = 0.0009. Scale bar shows 26 µm.

See also Figures S2, S7, S8, S11, and S13.

Fat2 intracellular domain is necessary for appropriate glomerular organization

Fat2 is predicted to function as a cell adhesion molecule, which upon trans interactions across neuronal membranes lead to cytoskeletal remodeling to support axonal fasciculation and axon terminal morphology.[33,43] To test whether the intracellular domain is required for Fat2 function in ORNs, we analyzed *fat2* mutants that encode a truncated Fat2 protein with the intracellular domain replaced with three copies of GFP ($fat2^{\Delta ICD}$). $Fat2^{\Delta ICD}$ mutants effectively phenocopy the *fat2* null mutants for Or47b, Or47a, and Or23a glomeruli (75% disrupted brains, n = 36) (Figures 1, 4A, and 4A′). This suggests signaling from Fat2 intracellular domain is required for Fat2 function during

glomerular organization. We further tested whether the intracellular domain of Fat2 was responsible for the ORN class-specific phenotypes (Figures 4B–4D′). Again, ORN classes with low Fat2 expression experienced little to no disruption in glomerular organization, whereas ORN classes with high Fat2 expression, exhibited strong disruptions. Notably, heterozygous *fat2*$^{\Delta ICD}$ mutants also display disruptions in glomerular morphology, not seen in *fat2* null heterozygous animals (*fat2*$^{\Delta ICD}$ heterozygous 62% phenotypic penetrance, *fat2* null heterozygous 17% phenotypic penetrance) (Figures 1D′ and 4A), suggesting possible dominant negative effects from Fat2$^{\Delta ICD}$ protein. In summary, the Fat2 intracellular domain plays a critical role in the Fat2 function as an organizer of ORN class-specific glomerular patterning.

To investigate whether the *fat2*$^{\Delta ICD}$-dependent phenotypic effect is due to protein mislocalization or loss of intracellular domain activity, we leveraged the three GFPs attached to *fat2*$^{\Delta ICD}$ protein to visualize the localization of the mutant protein in the brain and antennae (Figure S8B2). We found fluorescence signal in the commissure (red arrow), antennal lobe (pink arrow), and cell bodies adjacent to the antennal lobes (white arrows), but not in the antenna, in both *fat2-3xGFP* and *fat2*$^{\Delta ICD}$ (Figure S8). Therefore, we conclude there is no qualitative difference between *fat2-3xGFP* and *fat2*$^{\Delta ICD}$ mutant protein localization, even across developmental timepoints (Figures S8B1–S8B3). This suggests that the ICD mutant protein is not mis-localized, and likely maintains normal extracellular domain function.

Having established that Fat2 intracellular domain activity is necessary for appropriate in axon organization, we sought to identify which axon behavior is Fat2-dependent during glomerular formation. During olfactory circuit development ORN axons must perform several behaviors, including axon guidance toward the antennal lobe, axon targeting to the appropriate region within the antennal lobe, class-specific bundling to form proto-glomeruli, and lastly establishing synapses with second-order neurons to form a mature glomeruli.[8] To assess the impact of Fat2 on axon behavior during glomerular development, we aimed to identify the earliest developmental time point at which aberrant glomerular morphology can be visualized. Given that Fat2 expression begins at around 30 hAPF, we analyzed two time points after the onset of Fat2 expression. To perform the developmental analysis, we analyzed three glomeruli targeted by Or47a, Or47b, and Or23a ORNs at 48 hAPF and 72 hAPF. We found that at 48 hAPF, glomerular morphology was already disrupted for the three ORN classes (Figure 5A). Additionally, the disrupted glomerular morphology is maintained at 72 hAPF and into adulthood (Figure 5A) This suggests that glomerular morphology is likely stabilized by 48 hAPF and indicates that the phenotypes likely arose in earlier developmental time points. Since most *Or* genes are not expressed until 40 hAPF, we used an early developmental marker *72OK-GAL4* which strongly labels two Fat2-positive glomeruli (VM1 and VM4) and presents with glomerular defects in *fat2* mutants (Figures 3E and 3E′). *72OK-GAL4* driven *UAS-sytGFP* expression labels Ir92a (innervates VM1 glomerulus) and Ir76a (innervates VM4 glomerulus) ORNs within the first 15 hAPF.[4,42,44,45] This allows us to visualize general axon bundle dynamics from the earliest points of pupal stages through adulthood. We found that in control brains from 15 hAPF to about 22 hAPF the axon bundle penetrates the antennal lobe and extends ventral-laterally, likely in search of their target glomerular field. Once the axon bundle has reached the target region of the AL, around 25 hAPF, the axons condense (or is repelled from adjacent protoglomeruli) and coalesce with axons from the same ORN class into the spherical boundaries of VM1 protoglomerulus (Figure 5B). Around 30 hAPF there is a second phase of axon extension toward VM4 which also results in an irregularly shaped VM1 glomerulus. VM1 and VM4 glomerular morphology seems to stabilize after a second phase of axon condensation between 40 hAPF and 50 hAPF, after which glomerular morphology is stable until adulthood. Other publications document a similar series of axon behaviors in ORNs from other classes.[8]

The axon behaviors from 15 hAPF to around 25 hAPF are qualitatively analogous in mutants and control brains; however, the axon behaviors from older brains begin to deviate from controls more clearly. It is possible that early axon behaviors are affected, however, without high resolution single axon live imaging we are not able to discern any differences within the first 24 hAPF. Starting from approximately 25 hAPF, plus or minus 3 h, certain mutant brains displayed axon bundles with significant gaps within the anticipated glomerular field (Figures 5C3–5C5). In contrast, control brains exhibited a continuous axon bundle extending in the ventral-lateral direction. These large gaps within the axon bundles were observed in older brains but were absent in younger brains. It is important to note that it is unclear whether the absence of phenotypic disruptions in younger brains is due to the lack of a phenotypic effect or if higher resolution imaging is necessary to elucidate more nuanced disruptions to axon bundle architecture. Due to the similarities between these discontinuous axon bundles and the fragmentation seen in adult brains with the "split" phenotype, this aberrant axon bundle behavior may be a prerequisite to the "split" phenotype seen in adult *fat2* null brains. The other commonly seen aberrant axon bundle behavior is found as early as about 30 hAPF and is characterized by a premature halt in the ventral-lateral extension found in control brains at the same time frame (Figures 5C8 and 5C9). In earlier brains, we were not able to distinguish between whether the axon bundle had prematurely stopped or if it was in mid-development (Figure 5C7). In one phenotypic brain, the axon bundle seems to stop yet individual projections emerge from the bundle and continued projecting in all directions away from the axon bundle (Figure 5C9). This finding raises the possibility that axon bundle activity can be uncoupled from individual axon behavior, and that Fat2 activity may regulate axon bundle behavior but not necessarily impact individual axon behaviors. We would also like to note that the contralateral antennal lobes in the brains with prematurely halting axons, also presented with axon bundles that seem to behave more chaotically, and lacked the canonical globular morphology seen in age-matched control counterparts. Due to the visual similarities, we conclude this deviation in axon bundle behavior has the potential to relay the "rearranged" phenotype seen in the adult mutant brains. Notably, the 30–40 hAPF timepoint, when these aberrant axon bundle behaviors arise, coincides with the previously described onset of Fat2 expression within the antennal lobes (Figure S1).

In conclusion, *fat2* mutants disrupt axon behaviors during protoglomerular formation in early pupal development. We found that in *fat2* mutants, ORN axons lose the ability to organize into ORN class-specific protoglomerular fields.

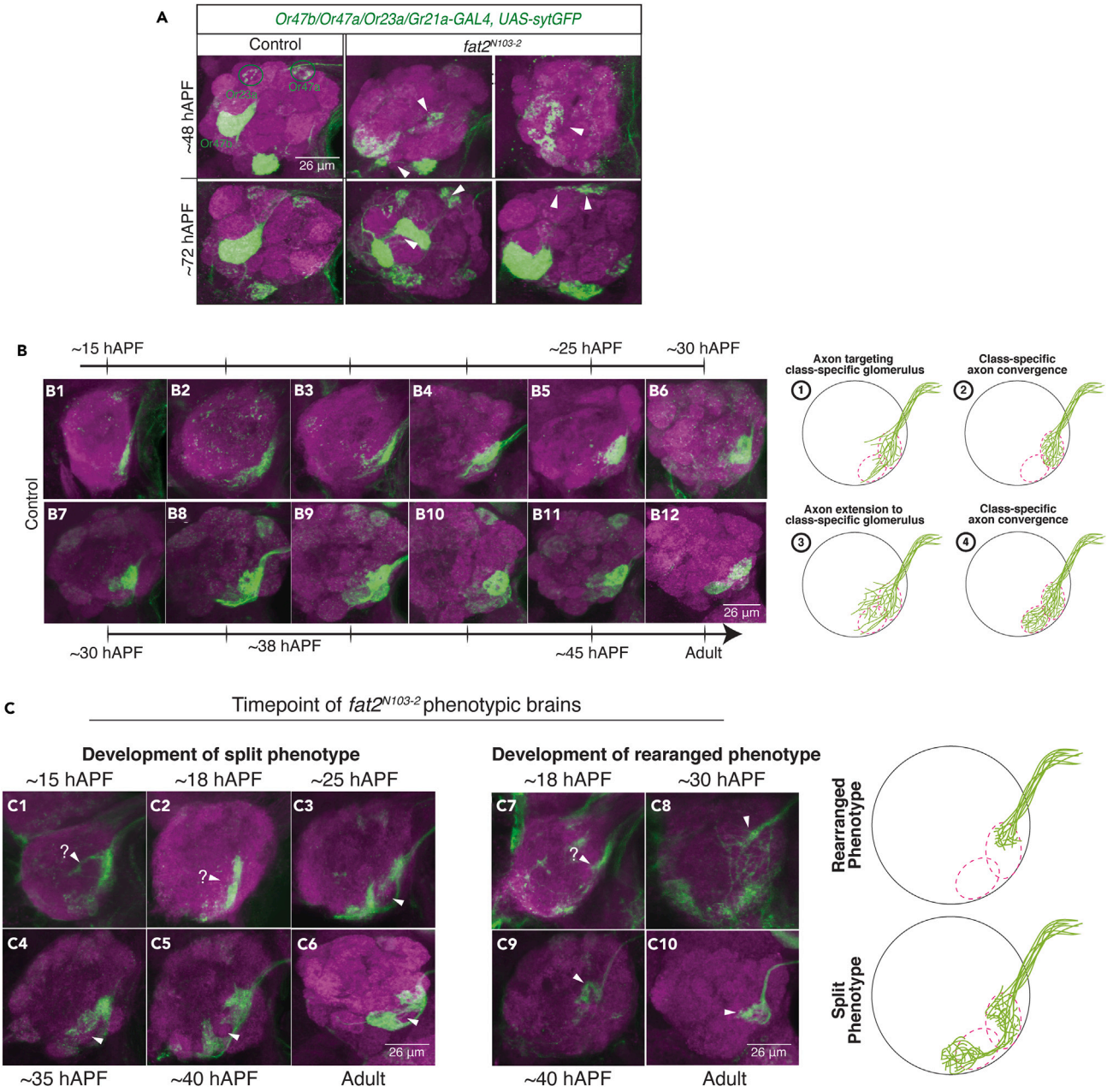

Figure 5. *fat2* mutant phenotype is apparent during protoglomerular development between 18 hAPF and 45 hAPF

(A) Representative images of control and *fat2*$^{N103-2}$ show three glomeruli corresponding to Or23a, Or47a, Or47 b at 48 hAPF (hours after pupal formation) and 72 hAPF, which corresponds to 50% and 75% pupal development respectively. Brains were stained with anti-GFP to visualize ORNs and with anti-N-Cadherin to visualize antennal lobe gross anatomy (magenta). White arrows point to disrupted glomerular morphology.

(B) Representative images of glomeruli labeled by *72OK-GAL4* driver in control brains between 15 hAPF and 45 hAPF. Developmental trajectory of *72OK-GAL4* axons shows two distinct extension phases, one from 15 hAPF to 25 hAPF and the second from 30 hAPF to 45 hAPF. By 45 hAPF, glomerular morphology closely resembles adult glomerular morphology. Schematic of axon organization during development. Black solid circle outline represents antennal lobe, magenta dashed ellipse outlines represent target glomeruli boundaries, green solid lines represent axonal processes.

(C) Representative images of *fat2*$^{N103-2}$ pupal brains speculated to result in either a "split" or "rearranged" phenotype. Brains between 18 hAPF and 45 hAPF visualizing axons labeled by *72OK-GAL4* (green) and N-Cadherin (magenta). (C1-C6) White arrow points to gap between glomeruli that is not present in control brains. (C7-C10) White arrow points to aberrant stunted axonal projections. White question marks with arrows point to axon bundle terminals at an early developmental time point where there is not enough detail to determine whether axon bundle behavior deviates from wildtype. Schematic of rearranged and split phenotypes. Scale bar shows 26 µm.

Projection neuron and local interneuron expression of Fat2 is not necessary for olfactory receptor neuron axon organization during glomerular development

Given that we found high *fat2* expressing cell bodies adjacent to the antennal lobes that likely project into the antennal lobes and interact with ORN axons, we set out to identify whether their expression is required for glomerular organization.[46] In the brains of transgenic animals expressing Fat2-3xGFP direct fusion proteins, we did find a population of Fat2-positive cells with cell bodies located adjacent to the antennal lobe and neurites projecting into the antennal lobes (Figures 2C and 2D). There are two known cell populations with cell bodies adjacent to the antennal lobe, projection neurons (PNs) and local interneurons (LNs).[45] To ascertain the neuronal identity of the Fat2-positive cell bodies, we conducted co-labeling experiments with specific markers for both PNs and LNs. By assessing the extent of cellular overlap, we aimed to identify the neuron type(s) associated with the Fat2-positive population. We first labeled a majority of PNs with *GH146-GAL4* driven expression of *10xUAS-RFP*[47] in the background of endogenous GFP-tagged Fat2 (Figure 6A). We saw minimal to no overlap between PNs and the Fat2-3xGFP signal (Figure 6A). Additionally, intersectional genetic systems that selectively label *fat2*-positive PNs revealed only one to three PN somas per antennal lobe innervating DM2 and VM2 glomeruli, which are innervated by Or22a and Or43b ORNs respectively (Figure S3). We also used *fat2-GAL4* to drive the expression of DenMark, a dendrite-specific marker that would highlight any glomeruli innervated by *fat2-GAL4*-positive PNs, if any (Figure S9).[48] We again found that *fat2*-positive dendrites were much fainter compared to the *GH146-GAL4*-labeling dendrites (Figure S3). Together, we used multiple genetic strategies to show that few PNs express Fat2 and glomerular Fat2 signal in the antennal lobes is not due to Fat2 localization to PN dendrites. Due to the little to no *fat2* expression in PNs, we can surmise that *fat2* expression by PNs is not required for ORN axon organization and glomerular morphology.

LNs also have cell bodies adjacent to the antennal lobe and project neuronal processes into the antennal lobe glomeruli. To positionally compare the *fat2*-positive somas to the cell bodies of several LNs subclasses,[49] we again co-labeled LN subclasses using LN-specific GAL4s driving *UAS-RFP* together with Fat2-3xGFP. We found only one LN subclass labeled by *499-GAL4* that overlapped with Fat2-3xGFP-positive cell bodies (Figure 6B). Given the proximity between LN axons and ORN axons, it is likely that Fat2 could regulate glomerular organization through mediating interactions between developing LN projection terminals and ORN axon terminals. To investigate this possibility, we knocked down *fat2* specifically in *499-GAL4*-positive LNs. We found no noticeable disruption to the axon organization for Or47b ORNs (Figure 6C), nor to the organization of LN processes (Figure S10). This suggests that LN's expression of Fat2 does not play a role in establishing glomerular morphology or ORN axon organization.

Together, our results revealed that outside of ORNs, Fat2 is also expressed in LN classes but not PNs within olfactory circuits. Yet LN expression of Fat2 is not required for its function in glomerular organization. Given that 1) Fat2 is predominantly expressed by ORNs and LNs and 2) only ORN-specific knockdown of *fat2* results in glomerular disruptions (Figures 1B and 1C), Fat2 mediated protoglomerular organization relies on Fat2 expression in ORN terminals to drive class-convergence conducive axon behaviors.

Fat2 intracellular domain orchestrates complex interactions with cytoskeletal regulators

To determine how Fat2-induced intracellular signaling conduct ORN axon behaviors critical to class-specific glomerular organization, we perturbed proteins that putatively interact with the Fat2 intracellular domain and analyzed their effects on the glomerular organization. To narrow down our target list, we used a recently generated dataset of mammalian Fat3-ICD interactors identified using protein pulldowns and mass spectrometry.[50] Among the 103 proteins in the dataset, we selected the top 10 potential interactors that had Drosophila orthologues with available RNAi genetic reagents to assess glomerular organization in knockdown conditions. *peb-GAL4* driven *UAS-RNAi* knockdown identified four of these genes (*Apc, CG17528* (*zyg8*), *chb*, and *dop*) phenocopied glomerular organization defects found in *fat2* mutants. We also confirmed the phenotype was not caused by the background effect associated with the *UAS-RNAi* transgene docking site (Figure S11), which may influence ORN glomerular organization based on our previous finding.[51]

Based on the literature *CG17528* and *Apc* play important roles in regulating actin and microtubule cytoskeleton, while *dop* encodes a kinase that regulates protein localization and transport.[52–66] If Fat2 intracellular domain indeed interacts with these proteins, we imagine that Fat2 gathers the appropriate cytoskeletal effectors to regulate the cytoskeletal framing of axon terminals and thus affect axon behavior. We further investigated whether any of these genes genetically interacted with *fat2* by asking if reducing the dose of *fat2* by half in the ORN-specific RNAi knockdown background enhanced or suppressed phenotypes observed (Figures 7A and 7B). This secondary screen identified *dop* and *Apc* RNAi knockdown glomerular phenotypes to be enhanced if they also carried a copy of *fat2* mutation (Figure 7A). On the other hand, *fat2* mutation mildly suppressed RNAi phenotypes observed in *zyg8/CG17528* knockdowns (Figures 7A and 7B). In addition to RNAi, we further validated these genetic interactions utilizing whole animal mutants for *dop* and *Apc*. Once again, we assessed the number of brains with disrupted glomerular organization when one copy of *dop*, *apc*, or *fat2* were disrupted and compared these heterozygotes with trans-heterozygotes where we halved *fat2* expression by introducing one copy of *fat2* null allele ($fat2^{N103\text{-}2}$) into *dop* or *Apc* heterozygotes. *dop* heterozygotes brains presented with few disruptions comparable to our controls (11% disrupted brains, 4/35 brains). When we added one copy of *fat2* null allele, we found a trending increase in the percentage of disrupted brains (21%, 7/33 brains, $p = 0.33$) (Figures 7C and 7D). The dop^{1} allele is known to be a hypomorph which produces the wildtype protein with a mutation in *dop* kinase domain leading to lowered/disrupted kinase activity.[60] This incomplete disruption of the *dop* protein could mask possible genetic interaction between *fat2* and *dop*. Therefore, further investigations are necessary to assess the trending increase in phenotypic penetrance for dop^{1}-$fat2^{N103\text{-}2}$ transheterozygotes. *Apc* and *Apc2* have been shown to play both mutually exclusive roles as well as redundant and synergistic roles.[67] Therefore, to account for compensation from *Apc2* we used a whole animal with null mutations in both Apc family members in order to test genetic interaction with Fat2. Mutants with one copy of Apc^{Q8} and $Apc2^{N175K}$ null alleles had a significantly higher rate of disrupted brains compared to

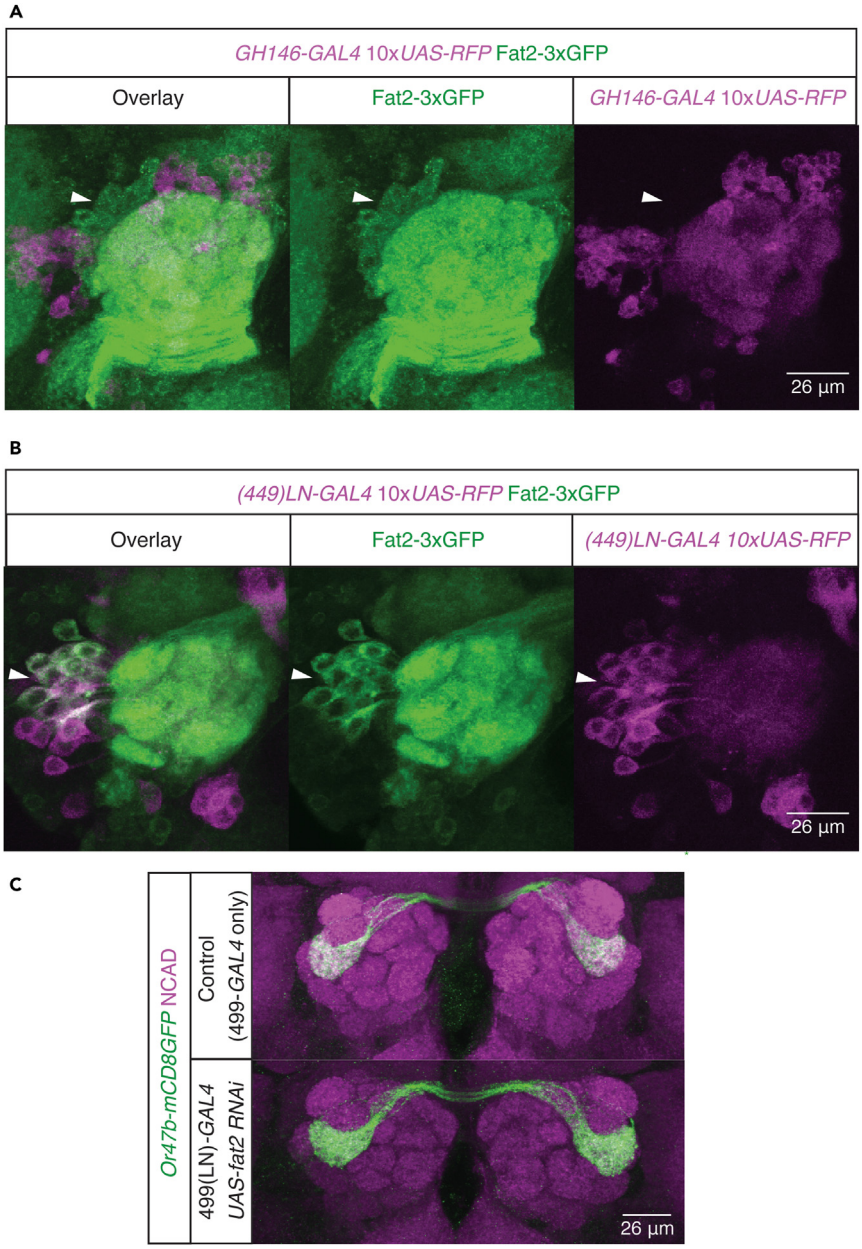

Figure 6. Local interneuron expression of *fat2* does not contribute to ORN glomerular organization

(A) Representative unstained z stack image of both antennal lobes where *GH146-GAL4*-labeled PNs in magenta and Fat2-3xGFP fusion protein in green. White arrows represent Fat2+ cell bodies that do not colocalize with PN cell bodies.

(B) Similar to panel A, Fat2-3xGFP fusion protein is colorized green and *499-GAL4* positive LNs are colorized magenta. White arrows represent Fat2+ cell bodies that colocalize with LN cell bodies.

(C) Representative z stack composite images of control antennal lobes and LN-specific knockdown of *fat2 (499-GAL4, UAS-fat2 RNAi)* stained with anti-N-Cadherin (magenta) and Or47b axons projecting into corresponding glomeruli (Green) stained with anti-GFP (*Or47b-GAL4, UAS-mCD8GFP*). Control brains presented with 1/18 brain with disruption (6% phenotypic penetrance), *499-GAL4 UAS-fat2 RNAi* presented with 1/16 brain with disruptions (5.75% phenotypic penetrance). Scale bar shows 26 µm.

See also Figures S9 and S10.

control (32%, 12/37 brains). Unlike dop^{1}-$fat2^{N103\text{-}2}$ transheterozygotes, $Apc^{Q8}Apc2^{N175K}$ with one copy of the *fat2* null allele was able to significantly rescue the phenotype seen in $Apc^{Q8}Apc2^{N175K}$ heterozygotes (11%, 4/35 brains). If Apc/Apc2 interacts with the intracellular domain of Fat2, then genetic interaction between $Apc^{Q8}Apc2^{N175K}$ and $fat2^{\Delta ICD}$ transheterozygotes should also significantly rescue the disrupted brain phenotype. Unlike $fat2^{N103}$ heterozygotes which does not present with any disruptions, $fat2^{\Delta ICD}$ heterozygotes do present with significant

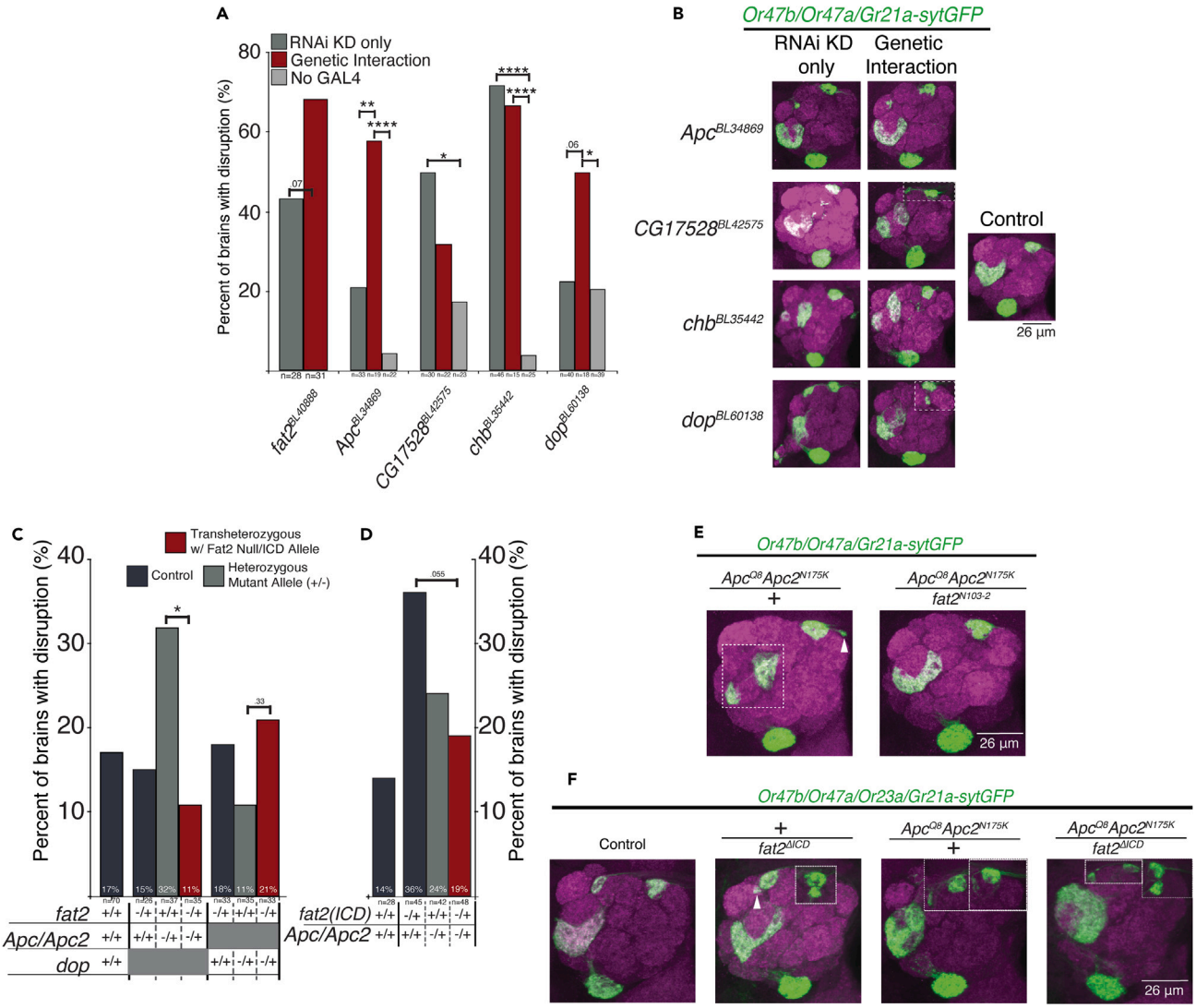

Figure 7. Testing genetic interactions with *fat2* by knocking down putative Fat3 intracellular domain interactors in sensitized *fat2* null heterozygous background

(A) Bar graph quantifying percentage of brains with disrupted glomerular morphology (in B) to test genetic interactions between *fat2* and the respective genes. Dark gray bar represents ORN-specific RNAi knockdown only for the denoted gene. Red bar represents RNAi knockdown of denoted gene in *fat2* null heterozygous background. Light gray bar represents control group with no *GAL4*, just *UAS-RNAi* in *fat2* null heterozygous background. *fat2* RNAi knockdown with and without one copy of $fat2^{N103\text{-}2}$ used as positive control (*p*-value calculated using fisher's exact, $p = 0.0695$). Generally, $*p < 0.05$, $**p < 0.01$, $****p < 0.0001$. Specifically, *Apc*, $**p = 0.0143$; *CG17528*, $*p = 0.0208$; *dop*, $*p = 0.0323$.

(B) Representative confocal z stack composite images of the disrupted glomeruli morphology seen in each group. Brains were stained with anti-N-Cadherin in magenta to visualize antennal lobe anatomy, and anti-GFP in green. Three ORN classes are labeled: Or47a, Or47b, and Gr21a. Dotted white boxes show overlay from another brain with representative disruptions to Or47a (or Gr21a) innervated glomerulus.

(C) Bar graph quantifying whole animal transheterozygote analysis of one copy of $dop(dop^{1})$ or $Apc/Apc2(Apc^{Q8}Apc2^{N175K})$ null allele with and without one copy of $fat2^{N103\text{-}2}$. Black bars represent two control conditions, gray bar represent *dop* or *Apc/Apc2* null heterozygotes, red bar represent transheterozygotes disrupting one copy of the gene of interest (*dop* and *Apc/Apc*) and one copy of *fat2*. Differences between red bar and gray bar suggest genetic interaction between the gene of interest and *fat2*. *p*-value calculated using fisher's exact, $*p = 0.0468$.

(D) Bar graph quantifying whole animal transheterozygote analysis of *Apc/Apc2* mutant with and without one copy of $fat2^{\Delta ICD}$.

(E) Representative images of glomerular disruptions found in specified genotypes. Dotted white boxes show overlay from another brain with representative disruptions to Or47b ORN innervated glomerulus, and white arrow points to fracturing glomerulus innervated by Or47a ORNs.

(F) Representative images of disrupted and control brains from the respective genotypes. Dotted white boxes show overlay from another brain with representative disruptions to Or47a and Or23a. White arrow pointing to fractured Or23a-innervated glomerulus. Scale bar shows 26 µm.

See also Figures S12 and S13.

aberrations in glomerular organization. Though not statistically significant by definition, with a *p*-value of 0.0557 calculated by Fisher's exact test, $Apc^{Q8}Apc2^{N175K}$ and $fat2^{\Delta ICD}$ transheterozygotes (19%, 9/49 brains disrupted) biologically significantly rescues the disruptions found in $fat2^{\Delta ICD}$ heterozygotes (36%, 16/29 brains disrupted) (Figures 7D and 7F). For Fat2 and Apc/Apc2 to physically interact they would have to be expressed within the same cells. To investigate whether *fat2* and *Apc/Apc2* were expressed by the same cells in the olfactory system, we analyzed available single-cell RNA-seq data to assess the class-specific expression levels for *fat2, Apc, and Apc2* during developmental stages (Figure S12). The RNA profiles suggest that *fat2* and *apc* are broadly expressed across Or-classes during pupal development. Notably, *Apc* is expressed at much lower levels compared to *fat2* expression levels. Given that *Apc* and *Apc2* encode proteins that play roles in multiple cell biological processes, it is unclear if Fat2 regulates Apc/Apc2's role in the regulation of β-catenin/Wingless signaling or the regulation of microtubule organization. The consistent genetic interaction between Fat2 and Apc/Apc2, strongly suggests that the mechanism of action for Fat2 relies on Fat2 intracellular domain interactions with intracellular regulators to achieve the desired ORN class-specific axon behavior. Additional research is necessary to precisely elucidate the underlying mechanisms, including whether Fat2 modulates Apc/Apc2 activity, localization, or both. Nonetheless, our study lays a solid foundation for understanding the nuanced role of Fat2 in orchestrating the class-specific axon behaviors in olfactory circuitry.

DISCUSSION

The olfactory sensory circuit possesses a distinctive feature present in nearly all neural circuits across the animal kingdom, namely its functionally organized topographic map. This map relies on widely dispersed neurons of the same type, which converge their axons into a neuropil called a glomerulus. The intricate process of how neuronal identity influences circuit organization is a significant area of research in neurobiology due to its close connection to neurodegeneration and neuronal dysfunction. Within the olfactory system, various cell surface proteins, such as Robo/Slit and Toll receptors, regulate many aspects of circuit organization, including axon guidance and synaptic matching. In this study, we have discovered an unconventional Cadherin protein called Fat2, which acts as a regulator of axon organization specific to certain classes. Fat2 exhibits the highest expression levels during metamorphosis, when the larval olfactory system disintegrates before re-constructing the mature olfactory circuit, with varying levels of Fat2 expression specific to each class. By studying *fat2* null mutants, we observed distinct effects on each class's glomerulus, with the most severely affected being those with the highest expression of fat2. Furthermore, we provide evidence suggesting that the intracellular domain of Fat2 is necessary for its function in organizing the axons of olfactory receptor neurons (ORNs). Examination of confocal images from early pupal development indicates that Fat2 is crucial for appropriate axon bundle behavior, which in turn allows for the correct spatial positioning and condensation of class-specific neuropils. Our research also indicates that the expression of Fat2 in projection neurons (PNs) and local interneurons (LNs) does not significantly contribute to the organization of ORNs. Finally, we have identified potential interactors of Fat2's intracellular domain that regulate ORN axon behavior, likely via coordinating the necessary cytoskeletal changes, during the early stages of glomerular development. In summary, our findings lay the groundwork for understanding the role of Fat2 in the organization of the olfactory circuit and highlight the critical importance of axon bundle behavior during the maturation of protoglomeruli.

Glomerular morphology relies on Fat2-dependent ORN axon behaviors

ORN axons arrive at the antennal lobes early in pupal development and undergo a sequence of processes: defasciculating and dispersal across AL, class-specific axon convergence to form protoglomerular bundles, followed by an intra-glomerular axon expansion, and finally secondary compaction of the axon terminals as glomeruli form boundaries and mature (Figure 5). These axonal behaviors are accompanied by cell surface protein mediated recognition of ORN-PN-LN terminals and dendrites to allow for proper synapse formation across these varying components of the antennal lobe glomeruli.[45] The developmental analysis of *fat2* mutants revealed that the major process that seems to be defective is the final stage of glomerular formation, wherein axon terminals collectively migrate as a class-specific bundle before spreading throughout the prospective glomerular field to establish a cohesive protoglomerulus. Specifically, this perturbation occurs when the bundle prematurely halts or when segments of the bundle disengage from the main bundle but nonetheless proceed to execute the remaining axon behaviors necessary for glomerular formation. As a consequence, these aberrant bundle behaviors lead to the emergence of gaps between glomerular fields that should ideally be contiguous, or a displacement from the stereotyped positioning/orientation. Coincidentally, another publication pinpointed this time frame (after the axon has innervated its target glomerulus) as a critical transition checkpoint for axon cytoskeletal organization. Specifically, the article found that prior to the innervation of the target glomerulus, axon branches contain predominantly microtubule networks with occasional actin filaments found in a minority of branches. However, after the axon innervates the target glomerulus, the axon will produce interstitial branches to innervate and spread through the glomerulus interior and these interstitial axon branches all contain both high actin network and microtubule network.[8] It is conceivable that Fat2 may be playing a role in this cytoskeletal reorganization post-innervation, possibly by localization APC (which is known to stabilize actin and microtubule networks) to axon terminals. One might hypothesize that the presence of two cytoskeletal networks leads to a stabilization of the axon branches that when disrupted can lead to axon instability and aberrant axon behaviors. However, further research is necessary to confirm whether cytoskeletal networks are differentially organized between control and Fat2 mutants. This phenotype differs from the function of N-Cadherin,[4] which mostly impacts the initial elaboration of axon terminals within glomeruli, suggesting the sequential utilization of different Cadherins in the stepwise progression of glomerular organization in the antennal lobes.

The pattern of Fat2 expression in the developing Drosophila brain shows very specific localization largely to ORNs and a subset of LNs, but not PNs. However, cell type-specific RNAi knockdowns of *fat2* are associated with glomerular defects only when Fat2 function is disrupted in

ORNs but not in LNs. In whole animal *fat2* mutants that exhibit glomerular defects, ORNs still retain their normal PN synaptic targets. These results suggest that Fat2 mainly functions to mediate ORN axon behaviors rather than establishing connection specificity with other neuronal components of olfactory circuit organization within antennal lobe glomeruli. Considering that Fat2's influence on ORN axon behaviors is sufficient to perturb glomerular morphology, the subsequent crucial step would involve determining whether Fat2 facilitates ORN-ORN interactions or if it primarily governs the cell-autonomous regulation of ORN axon terminals.

Circuit organization through Fat2 intracellular signaling function is conserved between flies and mammals

Across most neural circuits in any animal, axonal growth cones in developing neurons are highly dynamic and require tight regulation of the cytoskeleton to drive axon guidance, axon fasciculation, and synapse formation. Utilizing mass spectrometry, several publications have reported the identification of cytoskeletal proteins that interact with the intracellular domain of mammalian orthologue of the Drosophila Fat2 and Fat3 to regulate neuronal projection behaviors.[38,50] Utilizing RNAi in the background of *fat2* null heterozygotes, we found that axonal phenotypes found in *dop,* which regulates cytoskeletal organization and membrane growth, RNAi knockdown were enhanced by reducing the dose of *fat2*. In contrast, whole animal mutant analysis of *Apc/Apc2,* which encodes a β-catenin regulators/cytoskeletal anchors, resulted in a reduction of glomerular disruptions when *fat2* is disrupted in conjunction with *Apc/Apc2* disruption. These findings indicate that Fat3-ICD interactions in the developing mouse brain are conserved and mirrored with Fat2 in the developing insect brain. Utilizing Psi-BLAST, we performed an alignment between mouse Fat3 and drosophila Fat2 resulting in 95.2% coverage. We further annotated the mammalian Fat3 sequence for published binding motifs for Kif5, WIRS, and Evh1 (solid red rectangle). The Evh1 binding sites seem to not be conserved in drosophila Fat2 based on the lack of proline-rich sequence homology,[68] however several other regions of the ICD exhibit high sequence similarity (such as the putative PTB-like sequence YHWDxSDW, critical for Fat1 localization[69]), making them particularly promising candidates for future domain mutation investigations (Figure S13). Despite the lack of sequence alignment for WIRS binding sites, both mammalian Fat3[70] and drosophila Fat2 contain non-conserved WIRS binding sites[71] which demonstrates that functionality can be conserved without sequence homology. Even though no reports of the role of Fat3 function in mammalian olfactory circuit development, multiple sources confirm the high expression of Fat3 in the developing mouse olfactory bulb.[30,31,35,36] Given the intracellular interaction conservation and the high Fat3 expression in the developing olfactory bulb, Fat3-ICD is likely functionally relevant in the mammalian olfactory circuit development.

In contrast to the effects seen in the Fat3 intracellular domain mutants in mammals, which lead to the formation of an ectopic plexiform layer in the retina due to individual neurite retraction defects, the ORN class-specific glomerular splits, though sharing the characteristic of an ectopic neuropil, are attributed to abnormal axon bundle behavior — behavior not associated with the formation of retinal plexiform layers.[38,72] This difference in axonal phenotype, suggests Fat2 mechanism of action may not be conserved across sensory systems. It is still to be determined whether Fat2 mechanism of action is conserved in the same sensory system between mammals and insects. Nonetheless, as a protein that plays a regulatory role in multiple sensory systems with conserved protein interactions across species, Fat2, and it's mammalian orthologue, is likely instrumental to the organization of human neural circuits.

Aside from circuit organization, Fat2 might play a role in other neuronal processes as well. In mammals, the aberrant neurites failed to form mature synapses, suggesting defects in axon behaviors are accompanied by defects in synapse formation.[50] This finding provides a possible explanation for the ORN neurodegeneration seen in our *fat2* mutants since it is well accepted that disruptions to synaptogenesis/synaptic function can lead to regressive processes such as neurodegeneration.[73] Further studies are required to confirm whether ORN synaptic number is affected in *fat2* null animals.

Fat2 function in axon organization versus planar polarity

Previously, Fat2 function in Drosophila was predominantly proposed to be restricted to the regulation of planar cell polarity and collective cell migration.[25,27,74,75] In this article, we show that Fat2 function in neuronal development and ORN axon terminal organization depends on the intracellular domain, as *fat2* mutants with only the extracellular domain phenocopy null mutants. This contrasts with the planar cell polarity phenotypes in the egg chambers where the extracellular domain of Fat2 alone can partially rescue the mutant phenotypes observed in *fat2* null mutants. As an atypical Cadherin, Fat2 can mediate cell-cell adhesion, yet membrane proteins that act as ligands or receptors for Fat2 have not been identified. Recent studies have implicated putative roles for Sema5c or Lar as potential trans interactors of Fat2 in mediating planar polarity and collective cell migration in the egg chambers[74]; however, we were unable to detect genetic interactions in glomerular organization using mutations in either gene (data not shown). In addition, mutations in *Lar* exhibited phenotypes that were distinct from *fat2* mutants (data not shown). Therefore, these results suggest potential differences in mechanisms of Fat2 function in establishing planar cell polarity versus glomerular organization.

In addition to Fat2, another member of the family, Drosophila Fat cadherin, is a well-established regulator of growth and patterning via the Hippo pathway.[34,76] Despite their functional similarity, the intracellular domain of Fat and Fat2 are highly divergent and are much more similar to their mammalian orthologues, Fat4 and Fat3 respectively.[35,77] Furthermore, mammalian Fat1/Fat4 interaction can regulate aspects of neurodevelopment in mice.[78] Thus, the function of Fat protein family members in supporting neuronal survival might be conserved across protein family members and species, as *fat* mutants are associated with ommatidial degeneration in the Drosophila visual system.[79] It is unclear if Fat protein function in the nervous system extends outside of the visual system or interacts with Fat2 in axon terminal organization. Another future avenue to investigate is whether interactions between Fat2 and Fat, or other transmembrane receptors, drive olfactory circuit organization and neuronal survival.

Limitations of the study

Our analysis of *fat2* expression profile suggests high expression in the local interneurons[80] during olfactory circuit development. Yet, LN-specific knockdown of *fat2* did not impact ORN axon organization. Given that the scope of our research focuses on ORN class-specific regulation of ORN circuit topography, the role of Fat2 in LN development remains to be investigated. LNs play an integral role in modulating synaptic sensitivity to appropriately relay inter-glomerular and intra-glomerular signals.[81] Fat2 regulation of glomeruli morphology and expression in LNs, a key regulator of olfactory signal processing, raises the fundamental question as to whether *fat2* null flies exhibit behavioral defects. Behavioral analysis and electrophysiological evaluations of *fat2* null/ICD mutants or cell type-specific knockdown of *fat2* could elucidate possible neuro-pathologies related to *fat2* dysfunction. This could provide possible mechanistic insights into mutations in mammalian *fat3* associated with schizophrenia and bipolar disorder.[82]

While we have shown that the extracellular domain of Fat2 is not sufficient to rescue the fractured class-specific glomeruli, the extracellular domain of many cadherin proteins remains integral to their function, and Fat2 is likely no exception.[21] To directly investigate the role of Fat2 extracellular domain (*ECD*), we would need to generate a $fat2^{\Delta ECD}$ mutant with a functional intracellular domain and disrupted extracellular domain. However, due to the size of the extracellular domain, molecular cloning techniques to precisely remove the ECD have not been successful. Similarly, the generation of an insertion mutant, *UAS-fat2,* is difficult due to the sheer size of the *fat2* gene. A *GAL4* inducible *UAS-fat2* would be a powerful reagent because it would allow us to perform rescue experiments as well as over-expression analysis. Recent advances in gRNA-based overexpression using modified transcriptional activator CRISPR proteins can also be useful approaches for rescuing mutant phenotypes and overexpression experiments further probing Fat2 function.

Given that Fat2 likely functions during dynamic axon behaviors, available tools for inducible genetic disruptions, including conditional genetic drivers, may not be precise enough to assess Fat2 function. Furthermore, developmental trajectories of ORN classes are highly asynchronous and dependent on the birthdate of a given ORN class,[6] which means adjacent glomeruli can be at very different developmental stages at a given time point. Therefore, knocking down *fat2* at a specific time point might affect axon behaviors depending on the developmental phase of each ORN class.

A major limitation of our study is the absence of live single ORN axon imaging of wild-type and *fat2* mutants during olfactory system development. Our developmental analysis provides snapshots of axonal bundles to investigate general disruptions in axon behavior in *fat2* null mutants (Figure 5), in addition to the spatiotemporal expression profile for Fat2. This coarse perspective may obscure potential roles that Fat2 plays in more transient axon behaviors, as well as Fat2-dependent variations across single axons belonging to the same ORN class.

To summarize, one general organizational logic found in neural systems across various species is the arrangement of neurons performing similar functions to project to similar regions of the brain. Our results provide evidence for a conserved Fat2 function in organizing both the mammalian and insect circuit architecture, thus emphasizing the translational implications[83] of further research into Fat2 and the Fat cadherin family. Future live imaging approaches to ORN development will reveal a more dynamic view of the role of Fat2 in ORN axon behaviors. The results from these studies suggest that in addition to a combinatorial and differentially expressed cell surface receptor code, there likely is a combinatorial code of intracellular cytoskeletal effectors. Further investigation will be necessary to identify the mechanism behind Fat2-Apc/Apc2 interactions as well as validate Fat2-Dop interactions in driving ORN axon behaviors during circuit assembly. Once again, live imaging of Fat2 protein dynamics in conjunction with cytoskeletal markers or intracellular interactors during ORN development, in parallel with biochemical and targeted genetic approaches will establish mechanisms by which Fat2 governs ORN axon behaviors.

STAR★METHODS

Detailed methods are provided in the online version of this paper and include the following:

- KEY RESOURCES TABLE
- RESOURCE AVAILABILITY
  - Lead contact
  - Materials availability
  - Data and code availability
- EXPERIMENTAL MODEL AND STUDY PARTICIPANT DETAILS
  - Genetics, fly husbandry, and RNAi knockdown
- METHOD DETAILS
  - Immunohistochemistry and image acquisition
  - *72OK-GAL4* developmental time point analysis
- QUANTIFICATION AND STATISTICAL ANALYSIS
  - Phenotypic scoring
  - Fat2 protein expression analysis and intersectional labeling
  - Statistics
  - Analyzing the *fat2* expression in the single-cell RNA-seq datasets

SUPPLEMENTAL INFORMATION

Supplemental information can be found online at https://doi.org/10.1016/j.isci.2024.110340.

ACKNOWLEDGMENTS

We are grateful to Sally Horne-Badovinac for sharing *fat2* genetic reagents (as well as *sema5c* and *lar* mutants), and Christian Dahmann for sharing *fat2*^{58D} and other *fat2*-related fly lines. We want to thank Rachel Estrella, Douglas Blackiston, Julie Reynolds, Kavya Raghunathan, Latanya Coke, and Volkan lab members for their input on the article. We thank the Bloomington Stock Center for its services.

This study was supported by National Science Foundation award 2006471 to PCV and the National Science Foundation Graduate Research Fellowship under Grant No. DGE 2139754 to KMV.

AUTHOR CONTRIBUTIONS

Conceptualization: KMV and PCV. Investigation: KMV and CY with QD generating Figure 2A; Figures S11 and S12. SB contributed to the initial RNAi screen for cell surface receptors that revealed fat2 phenotype in ORNs. Analysis/interpretation of data: KMV, QD, and PCV. Article-original draft: KMV, QD, and PCV. Article-revision: KMV, QD, and PCV..

DECLARATION OF INTERESTS

The authors declare that they have no competing interests.

DECLARATION OF AI AND AI-ASSISTED TECHNOLOGIES IN WRITING PROCESS

During the writing of this article the author(s) used ChatGPT3 in order to increase readability and brevity, as well as correct grammatical errors. After using the tool/service the author(s) reviewed the edited the content as needed and take full responsibility for the contents of the publication.

Received: December 5, 2023
Revised: April 8, 2024
Accepted: June 19, 2024
Published: June 21, 2024

REFERENCES

1. Laissue, P.P., and Vosshall, L.B. (2008). The olfactory sensory map in Drosophila. Adv. Exp. Med. Biol. *628*, 102–114. https://doi.org/10.1007/978-0-387-78261-4_7.
2. Gao, Q., Yuan, B., and Chess, A. (2000). Convergent projections of Drosophila olfactory neurons to specific glomeruli in the antennal lobe. Nat. Neurosci. *3*, 780–785. https://doi.org/10.1038/77680.
3. Task, D., Lin, C.C., Vulpe, A., Afify, A., Ballou, S., Brbic, M., Schlegel, P., Raji, J., Jefferis, G.S.X.E., Li, H., et al. (2022). Chemoreceptor co-expression in Drosophila melanogaster olfactory neurons. Elife *11*, e72599. https://doi.org/10.7554/eLife.72599.
4. Hummel, T., and Zipursky, S.L. (2004). Afferent induction of olfactory glomeruli requires N-cadherin. Neuron *42*, 77–88. https://doi.org/10.1016/s0896-6273(04)00158-8.
5. Barish, S., Nuss, S., Strunilin, I., Bao, S., Mukherjee, S., Jones, C.D., and Volkan, P.C. (2018). Combinations of DIPs and Dprs control organization of olfactory receptor neuron terminals in Drosophila. PLoS Genet. *14*, e1007560. https://doi.org/10.1371/journal.pgen.1007560.
6. Barish, S., and Volkan, P.C. (2015). Mechanisms of olfactory receptor neuron specification in Drosophila. Wiley Interdiscip. Rev. Dev. Biol. *4*, 609–621. https://doi.org/10.1002/wdev.197.
7. Joo, W.J., Sweeney, L.B., Liang, L., and Luo, L. (2013). Linking cell fate, trajectory choice, and target selection: genetic analysis of Sema-2b in olfactory axon targeting. Neuron *78*, 673–686. https://doi.org/10.1016/j.neuron.2013.03.022.
8. Li, T., Fu, T.M., Wong, K.K.L., Li, H., Xie, Q., Luginbuhl, D.J., Wagner, M.J., Betzig, E., and Luo, L. (2021). Cellular bases of olfactory circuit assembly revealed by systematic time-lapse imaging. Cell *184*, 5107–5121.e14. https://doi.org/10.1016/j.cell.2021.08.030.
9. Hummel, T., Vasconcelos, M.L., Clemens, J.C., Fishilevich, Y., Vosshall, L.B., and Zipursky, S.L. (2003). Axonal targeting of olfactory receptor neurons in Drosophila is controlled by Dscam. Neuron *37*, 221–231. https://doi.org/10.1016/s0896-6273(02)01183-2.
10. Jhaveri, D., Saharan, S., Sen, A., and Rodrigues, V. (2004). Positioning sensory terminals in the olfactory lobe of Drosophila by Robo signaling. Development *131*, 1903–1912. https://doi.org/10.1242/dev.01083.
11. Ward, A., Hong, W., Favaloro, V., and Luo, L. (2015). Toll receptors instruct axon and dendrite targeting and participate in synaptic partner matching in a Drosophila olfactory circuit. Neuron *85*, 1013–1028. https://doi.org/10.1016/j.neuron.2015.02.003.
12. Kaur, R., Surala, M., Hoger, S., Grössmann, N., Grimm, A., Timaeus, L., Kallina, W., and Hummel, T. (2019). Pioneer interneurons instruct bilaterality in the Drosophila olfactory sensory map. Sci. Adv. *5*, eaaw5537. https://doi.org/10.1126/sciadv.aaw5537.
13. Lattemann, M., Zierau, A., Schulte, C., Seidl, S., Kuhlmann, B., and Hummel, T. (2007). Semaphorin-1a controls receptor neuron-specific axonal convergence in the primary olfactory center of Drosophila. Neuron *53*, 169–184. https://doi.org/10.1016/j.neuron.2006.12.024.
14. Sweeney, L.B., Chou, Y.H., Wu, Z., Joo, W., Komiyama, T., Potter, C.J., Kolodkin, A.L., Garcia, K.C., and Luo, L. (2011). Secreted semaphorins from degenerating larval ORN axons direct adult projection neuron dendrite targeting. Neuron *72*, 734–747. https://doi.org/10.1016/j.neuron.2011.09.026.
15. Goyal, G., Zierau, A., Lattemann, M., Bergkirchner, B., Javorski, D., Kaur, R., and Hummel, T. (2019). Inter-axonal recognition organizes Drosophila olfactory map formation. Sci. Rep. *9*, 11554. https://doi.org/10.1038/s41598-019-47924-9.
16. Zipursky, S.L., and Sanes, J.R. (2010). Chemoaffinity revisited: dscams, protocadherins, and neural circuit assembly. Cell *143*, 343–353. https://doi.org/10.1016/j.cell.2010.10.009.
17. Hong, W., Mosca, T.J., and Luo, L. (2012). Teneurins instruct synaptic partner matching in an olfactory map. Nature *484*, 201–207. https://doi.org/10.1038/nature10926.
18. Mosca, T.J., and Luo, L. (2014). Synaptic organization of the Drosophila antennal lobe and its regulation by the Teneurins. Elife *3*, e03726. https://doi.org/10.7554/eLife.03726.
19. Hong, W., and Luo, L. (2014). Genetic control of wiring specificity in the fly olfactory system. Genetics *196*, 17–29. https://doi.org/10.1534/genetics.113.154336.
20. Ryan, T.J., and Grant, S.G.N. (2009). The origin and evolution of synapses. Nat. Rev. Neurosci. *10*, 701–712. https://doi.org/10.1038/nrn2717.
21. Hirano, S., and Takeichi, M. (2012). Cadherins in brain morphogenesis and wiring. Physiol. Rev. *92*, 597–634. https://doi.org/10.1152/physrev.00014.2011.
22. Hasegawa, S., Hamada, S., Kumode, Y., Esumi, S., Katori, S., Fukuda, E., Uchiyama, Y., Hirabayashi, T., Mombaerts, P., and Yagi, T. (2008). The protocadherin-alpha family is involved in axonal coalescence of olfactory sensory neurons into glomeruli of the olfactory bulb in mouse. Mol. Cell. Neurosci.

38, 66–79. https://doi.org/10.1016/j.mcn.2008.01.016.

23. Hulpiau, P., and van Roy, F. (2011). New insights into the evolution of metazoan cadherins. Mol. Biol. Evol. *28*, 647–657. https://doi.org/10.1093/molbev/msq233.
24. Takeichi, M. (2007). The cadherin superfamily in neuronal connections and interactions. Nat. Rev. Neurosci. *8*, 11–20. https://doi.org/10.1038/nrn2043.
25. Horne-Badovinac, S., Hill, J., Gerlach, G., 2nd, Menegas, W., and Bilder, D. (2012). A screen for round egg mutants in Drosophila identifies tricornered, furry, and misshapen as regulators of egg chamber elongation. G3 (Bethesda) *2*, 371–378. https://doi.org/10.1534/g3.111.001677.
26. Aurich, F., and Dahmann, C. (2016). A Mutation in fat2 Uncouples Tissue Elongation from Global Tissue Rotation. Cell Rep. *14*, 2503–2510. https://doi.org/10.1016/j.celrep.2016.02.044.
27. Barlan, K., Cetera, M., and Horne-Badovinac, S. (2017). Fat2 and Lar Define a Basally Localized Planar Signaling System Controlling Collective Cell Migration. Dev. Cell *40*, 467–477.e5. https://doi.org/10.1016/j.devcel.2017.02.003.
28. Down, M., Power, M., Smith, S.I., Ralston, K., Spanevello, M., Burns, G.F., and Boyd, A.W. (2005). Cloning and expression of the large zebrafish protocadherin gene, Fat. Gene Expr. Patterns *5*, 483–490. https://doi.org/10.1016/j.modgep.2004.12.005.
29. Tanoue, T., and Takeichi, M. (2005). New insights into Fat cadherins. J. Cell Sci. *118*, 2347–2353. https://doi.org/10.1242/jcs.02398.
30. Mitsui, K., Nakajima, D., Ohara, O., and Nakayama, M. (2002). Mammalian fat3: a large protein that contains multiple cadherin and EGF-like motifs. Biochem. Biophys. Res. Commun. *290*, 1260–1266. https://doi.org/10.1006/bbrc.2002.6338.
31. Nagae, S., Tanoue, T., and Takeichi, M. (2007). Temporal and spatial expression profiles of the Fat3 protein, a giant cadherin molecule, during mouse development. Dev. Dyn. *236*, 534–543. https://doi.org/10.1002/dvdy.21030.
32. McLaughlin, C.N., Brbic, M., Xie, Q., Li, T., Horns, F., Kolluru, S.S., Kebschull, J.M., Vacek, D., Xie, A., Li, J., et al. (2021). Single-cell transcriptomes of developing and adult olfactory receptor neurons in Drosophila. Elife *10*, e63856. https://doi.org/10.7554/eLife.63856.
33. Aviles, E.C., and Goodrich, L.V. (2017). Configuring a robust nervous system with Fat cadherins. Semin. Cell Dev. Biol. *69*, 91–101. https://doi.org/10.1016/j.semcdb.2017.06.001.
34. Fulford, A.D., and McNeill, H. (2020). Fat/Dachsous family cadherins in cell and tissue organisation. Curr. Opin. Cell Biol. *62*, 96–103. https://doi.org/10.1016/j.ceb.2019.10.006.
35. Rock, R., Schrauth, S., and Gessler, M. (2005). Expression of mouse dchs1, fjx1, and fat-j suggests conservation of the planar cell polarity pathway identified in Drosophila. Dev. Dyn. *234*, 747–755. https://doi.org/10.1002/dvdy.20515.
36. Cheng, H., Burroughs-Garcia, J., Birkness, J.E., Trinidad, J.C., and Deans, M.R. (2016). Disparate Regulatory Mechanisms Control Fat3 and P75NTR Protein Transport through a Conserved Kif5-Interaction Domain. PLoS One *11*, e0165519. https://doi.org/10.1371/journal.pone.0165519.
37. Saburi, S., Hester, I., Goodrich, L., and McNeill, H. (2012). Functional interactions between Fat family cadherins in tissue morphogenesis and planar polarity. Development *139*, 1806–1820. https://doi.org/10.1242/dev.077461.
38. Krol, A., Henle, S.J., and Goodrich, L.V. (2016). Fat3 and Ena/VASP proteins influence the emergence of asymmetric cell morphology in the developing retina. Development *143*, 2172–2182. https://doi.org/10.1242/dev.133678.
39. Viktorinova, I., Konig, T., Schlichting, K., and Dahmann, C. (2009). The cadherin Fat2 is required for planar cell polarity in the Drosophila ovary. Development *136*, 4123–4132. https://doi.org/10.1242/dev.039099.
40. Li, J., Han, S., Li, H., Udeshi, N.D., Svinkina, T., Mani, D.R., Xu, C., Guajardo, R., Xie, Q., Li, T., et al. (2020). Cell-Surface Proteomic Profiling in the Fly Brain Uncovers Wiring Regulators. Cell *180*, 373–386.e15. https://doi.org/10.1016/j.cell.2019.12.029.
41. Silbering, A.F., Rytz, R., Grosjean, Y., Abuin, L., Ramdya, P., Jefferis, G.S.X.E., and Benton, R. (2011). Complementary function and integrated wiring of the evolutionarily distinct Drosophila olfactory subsystems. J. Neurosci. *31*, 13357–13375. https://doi.org/10.1523/JNEUROSCI.2360-11.2011.
42. Benton, R., Vannice, K.S., Gomez-Diaz, C., and Vosshall, L.B. (2009). Variant ionotropic glutamate receptors as chemosensory receptors in Drosophila. Cell *136*, 149–162. https://doi.org/10.1016/j.cell.2008.12.001.
43. Schmitz, C., Wacker, I., and Hutter, H. (2008). The Fat-like cadherin CDH-4 controls axon fasciculation, cell migration and hypodermis and pharynx development in Caenorhabditis elegans. Dev. Biol. *316*, 249–259. https://doi.org/10.1016/j.ydbio.2008.01.024.
44. Acebes, A., and Ferrús, A. (2001). Increasing the number of synapses modifies olfactory perception in Drosophila. J. Neurosci. *21*, 6264–6273. https://doi.org/10.1523/JNEUROSCI.21-16-06264.2001.
45. Grabe, V., Baschwitz, A., Dweck, H.K.M., Lavista-Llanos, S., Hansson, B.S., and Sachse, S. (2016). Elucidating the Neuronal Architecture of Olfactory Glomeruli in the Drosophila Antennal Lobe. Cell Rep. *16*, 3401–3413. https://doi.org/10.1016/j.celrep.2016.08.063.
46. Nakayama, M., Nakajima, D., Yoshimura, R., Endo, Y., and Ohara, O. (2002). MEGF1/fat2 proteins containing extraordinarily large extracellular domains are localized to thin parallel fibers of cerebellar granule cells. Mol. Cell. Neurosci. *20*, 563–578. https://doi.org/10.1006/mcne.2002.1146.
47. Jefferis, G.S., Marin, E.C., Stocker, R.F., and Luo, L. (2001). Target neuron prespecification in the olfactory map of Drosophila. Nature *414*, 204–208. https://doi.org/10.1038/35102574.
48. Nicolai, L.J., Ramaekers, A., Raemaekers, T., Drozdzecki, A., Mauss, A.S., Yan, J., Landgraf, M., Annaert, W., and Hassan, B.A. (2010). Genetically encoded dendritic marker sheds light on neuronal connectivity in Drosophila. Proc. Natl. Acad. Sci. USA *107*, 20553–20558. https://doi.org/10.1073/pnas.1010198107.
49. Liou, N.F., Lin, S.H., Chen, Y.J., Tsai, K.T., Yang, C.J., Lin, T.Y., Wu, T.H., Lin, H.J., Chen, Y.T., Gohl, D.M., et al. (2018). Diverse populations of local interneurons integrate into the Drosophila adult olfactory circuit. Nat. Commun. *9*, 2232. https://doi.org/10.1038/s41467-018-04675-x.
50. Aviles, E.C., Krol, A., Henle, S.J., Burroughs-Garcia, J., Deans, M.R., and Goodrich, L.V. (2022). Fat3 acts through independent cytoskeletal effectors to coordinate asymmetric cell behaviors during polarized circuit assembly. Cell Rep. *38*, 110307. https://doi.org/10.1016/j.celrep.2022.110307.
51. Duan, Q., Estrella, R., Carson, A., Chen, Y., and Volkan, P.C. (2023). The effect of Drosophila attP40 background on the glomerular organization of Or47b olfactory receptor neurons. G3 (Bethesda) *13*, jkad022. https://doi.org/10.1093/g3journal/jkad022.
52. Lee, H., Engel, U., Rusch, J., Scherrer, S., Sheard, K., and Van Vactor, D. (2004). The microtubule plus end tracking protein Orbit/MAST/CLASP acts downstream of the tyrosine kinase Abl in mediating axon guidance. Neuron *42*, 913–926. https://doi.org/10.1016/j.neuron.2004.05.020.
53. McKee, A.E., Minet, E., Stern, C., Riahi, S., Stiles, C.D., and Silver, P.A. (2005). A genome-wide *in situ* hybridization map of RNA-binding proteins reveals anatomically restricted expression in the developing mouse brain. BMC Dev. Biol. *5*, 14. https://doi.org/10.1186/1471-213X-5-14.
54. Kozlova, N., Braga, J., Lundgren, J., Rino, J., Young, P., Carmo-Fonseca, M., and Visa, N. (2006). Studies on the role of NonA in mRNA biogenesis. Exp. Cell Res. *312*, 2619–2630. https://doi.org/10.1016/j.yexcr.2006.04.013.
55. Nathke, I. (2006). Cytoskeleton out of the cupboard: colon cancer and cytoskeletal changes induced by loss of APC. Nat. Rev. Cancer *6*, 967–974. https://doi.org/10.1038/nrc2010.
56. Barth, A.I.M., Caro-Gonzalez, H.Y., and Nelson, W.J. (2008). Role of adenomatous polyposis coli (APC) and microtubules in directional cell migration and neuronal polarization. Semin. Cell Dev. Biol. *19*, 245–251. https://doi.org/10.1016/j.semcdb.2008.02.003.
57. Hur, E.M., Saijilafu, Lee, B.D., Kim, S.J., Xu, W.L., and Zhou, F.Q. (2011). GSK3 controls axon growth via CLASP-mediated regulation of growth cone microtubules. Genes Dev. *25*, 1968–1981. https://doi.org/10.1101/gad.17015911.
58. Bellanger, J.M., Cueva, J.G., Baran, R., Tang, G., Goodman, M.B., and Debant, A. (2012). The doublecortin-related gene zyg-8 is a microtubule organizer in Caenorhabditis elegans neurons. J. Cell Sci. *125*, 5417–5427. https://doi.org/10.1242/jcs.108381.
59. Koch, N., Dharmalingam, E., Westermann, M., Qualmann, B., Thomas, U., and Kessels, M.M. (2012). Abp1 utilizes the Arp2/3 complex activator Scar/WAVE in bristle development. J. Cell Sci. *125*, 3578–3589. https://doi.org/10.1242/jcs.101451.
60. Hain, D., Langlands, A., Sonnenberg, H.C., Bailey, C., Bullock, S.L., and Müller, H.A.J. (2014). The Drosophila MAST kinase Drop out is required to initiate membrane compartmentalisation during cellularisation and regulates dynein-based transport. Development *141*, 2119–2130. https://doi.org/10.1242/dev.104711.
61. Koch, N., Kobler, O., Thomas, U., Qualmann, B., and Kessels, M.M. (2014). Terminal axonal arborization and synaptic bouton formation critically rely on abp1 and the arp2/3 complex. PLoS One *9*, e97692. https://doi.org/10.1371/journal.pone.0097692.

62. Nawabi, H., Belin, S., Cartoni, R., Williams, P.R., Wang, C., Latremolière, A., Wang, X., Zhu, J., Taub, D.G., Fu, X., et al. (2015). Doublecortin-Like Kinases Promote Neuronal Survival and Induce Growth Cone Reformation via Distinct Mechanisms. Neuron *88*, 704–719. https://doi.org/10.1016/j.neuron.2015.10.005.
63. Barr, J., Charania, S., Gilmutdinov, R., Yakovlev, K., Shidlovskii, Y., and Schedl, P. (2019). The CPEB translational regulator, Orb, functions together with Par proteins to polarize the Drosophila oocyte. PLoS Genet. *15*, e1008012. https://doi.org/10.1371/journal.pgen.1008012.
64. Popow, O., Paulo, J.A., Tatham, M.H., Volk, M.S., Rojas-Fernandez, A., Loyer, N., Newton, I.P., Januschke, J., Haigis, K.M., and Näthke, I. (2019). Identification of Endogenous Adenomatous Polyposis Coli Interaction Partners and beta-Catenin-Independent Targets by Proteomics. Mol. Cancer Res. *17*, 1828–1841. https://doi.org/10.1158/1541-7786.MCR-18-1154.
65. Sayas, C.L., Basu, S., van der Reijden, M., Bustos-Morán, E., Liz, M., Sousa, M., van IJcken, W.F.J., Avila, J., and Galjart, N. (2019). Distinct Functions for Mammalian CLASP1 and -2 During Neurite and Axon Elongation. Front. Cell. Neurosci. *13*, 5. https://doi.org/10.3389/fncel.2019.00005.
66. Deng, S., Silimon, R.L., Balakrishnan, M., Bothe, I., Juros, D., Soffar, D.B., and Baylies, M.K. (2021). The actin polymerization factor Diaphanous and the actin severing protein Flightless I collaborate to regulate sarcomere size. Dev. Biol. *469*, 12–25. https://doi.org/10.1016/j.ydbio.2020.09.014.
67. Ahmed, Y., Nouri, A., and Wieschaus, E. (2002). Drosophila Apc1 and Apc2 regulate Wingless transduction throughout development. Development *129*, 1751–1762. https://doi.org/10.1242/dev.129.7.1751.
68. Moeller, M.J., Soofi, A., Braun, G.S., Li, X., Watzl, C., Kriz, W., and Holzman, L.B. (2004). Protocadherin FAT1 binds Ena/VASP proteins and is necessary for actin dynamics and cell polarization. EMBO J. *23*, 3769–3779. https://doi.org/10.1038/sj.emboj.7600380.
69. Braun, G.S., Kretzler, M., Heider, T., Floege, J., Holzman, L.B., Kriz, W., and Moeller, M.J. (2007). Differentially spliced isoforms of FAT1 are asymmetrically distributed within migrating cells. J. Biol. Chem. *282*, 22823–22833. https://doi.org/10.1074/jbc.M701758200.
70. Chen, B., Brinkmann, K., Chen, Z., Pak, C.W., Liao, Y., Shi, S., Henry, L., Grishin, N.V., Bogdan, S., and Rosen, M.K. (2014). The WAVE regulatory complex links diverse receptors to the actin cytoskeleton. Cell *156*, 195–207. https://doi.org/10.1016/j.cell.2013.11.048.
71. Squarr, A.J., Brinkmann, K., Chen, B., Steinbacher, T., Ebnet, K., Rosen, M.K., and Bogdan, S. (2016). Fat2 acts through the WAVE regulatory complex to drive collective cell migration during tissue rotation. J. Cell Biol. *212*, 591–603. https://doi.org/10.1083/jcb.201508081.
72. Deans, M.R., Krol, A., Abraira, V.E., Copley, C.O., Tucker, A.F., and Goodrich, L.V. (2011). Control of neuronal morphology by the atypical cadherin Fat3. Neuron *71*, 820–832. https://doi.org/10.1016/j.neuron.2011.06.026.
73. Brady, S., and Morfini, G. (2010). A perspective on neuronal cell death signaling and neurodegeneration. Mol. Neurobiol. *42*, 25–31. https://doi.org/10.1007/s12035-010-8128-2.
74. Stedden, C.G., Menegas, W., Zajac, A.L., Williams, A.M., Cheng, S., Özkan, E., and Horne-Badovinac, S. (2019). Planar-Polarized Semaphorin-5c and Plexin A Promote the Collective Migration of Epithelial Cells in Drosophila. Curr. Biol. *29*, 908–920.e6. https://doi.org/10.1016/j.cub.2019.01.049.
75. Williams, A.M., Donoughe, S., Munro, E., and Horne-Badovinac, S. (2022). Fat2 polarizes the WAVE complex in trans to align cell protrusions for collective migration. Elife *11*, e78343. https://doi.org/10.7554/eLife.78343.
76. Sopko, R., and McNeill, H. (2009). The skinny on Fat: an enormous cadherin that regulates cell adhesion, tissue growth, and planar cell polarity. Curr. Opin. Cell Biol. *21*, 717–723. https://doi.org/10.1016/j.ceb.2009.07.001.
77. Katoh, Y., and Katoh, M. (2006). Comparative integromics on FAT1, FAT2, FAT3 and FAT4. Int. J. Mol. Med. *18*, 523–528.
78. Badouel, C., Zander, M.A., Liscio, N., Bagherie-Lachidan, M., Sopko, R., Coyaud, E., Raught, B., Miller, F.D., and McNeill, H. (2015). Fat1 interacts with Fat4 to regulate neural tube closure, neural progenitor proliferation and apical constriction during mouse brain development. Development *142*, 2781–2791. https://doi.org/10.1242/dev.123539.
79. Napoletano, F., Occhi, S., Calamita, P., Volpi, V., Blanc, E., Charroux, B., Royet, J., and Fanto, M. (2011). Polyglutamine Atrophin provokes neurodegeneration in Drosophila by repressing fat. EMBO J. *30*, 945–958. https://doi.org/10.1038/emboj.2011.1.
80. Grando, S.A., Bystryn, J.C., Chernyavsky, A.I., Frusić-Zlotkin, M., Gniadecki, R., Lotti, R., Milner, Y., Pittelkow, M.R., and Pincelli, C. (2009). Apoptolysis: a novel mechanism of skin blistering in pemphigus vulgaris linking the apoptotic pathways to basal cell shrinkage and suprabasal acantholysis. Exp. Dermatol. *18*, 764–770. https://doi.org/10.1111/j.1600-0625.2009.00934.x.
81. Fusca, D., and Kloppenburg, P. (2021). Task-specific roles of local interneurons for inter- and intraglomerular signaling in the insect antennal lobe. Elife *10*, e65217. https://doi.org/10.7554/eLife.65217.
82. Blair, I.P., Chetcuti, A.F., Badenhop, R.F., Scimone, A., Moses, M.J., Adams, L.J., Craddock, N., Green, E., Kirov, G., Owen, M.J., et al. (2006). Positional cloning, association analysis and expression studies provide convergent evidence that the cadherin gene FAT contains a bipolar disorder susceptibility allele. Mol. Psychiatry *11*, 372–383. https://doi.org/10.1038/sj.mp.4001784.
83. Zhao, B., Luo, T., Li, T., Li, Y., Zhang, J., Shan, Y., Wang, X., Yang, L., Zhou, F., Zhu, Z., et al. (2019). Genome-wide association analysis of 19,629 individuals identifies variants influencing regional brain volumes and refines their genetic co-architecture with cognitive and mental health traits. Nat. Genet. *51*, 1637–1644. https://doi.org/10.1038/s41588-019-0516-6.
84. Fishilevich, E., and Vosshall, L.B. (2005). Genetic and functional subdivision of the Drosophila antennal lobe. Curr. Biol. *15*, 1548–1553. https://doi.org/10.1016/j.cub.2005.07.066.

STAR★METHODS

KEY RESOURCES TABLE

REAGENT or RESOURCE	SOURCE	IDENTIFIER
Antibodies		
Goat anti-Rabbit IgG (H+L) Highly absorbed secondary antibody, Alexa Fluor Plus 488 (1:1000)	Invitrogen	Ref:A32731 Lot:XH353659; RRID: AB_2633280
Alexa Fluor 546 goat anti-mouse IgG (H+L) (1:300)	Invitrogen	Ref:A11030 Lot:2273717; RRID: AB_2737024
Anti-green fluorescent protein, rabbit IgG fraction (1:1000)	Invitrogen	Ref:A11122 Lot:2477546; RRID: AB_221569
Rat anti-NCAD (1:20)	DSHB	Cat #: DN-Ex #8; RRID: AB_528121
Mouse anti-rat CD2 (1:500)	BioRAD	MCA154R Batch No:1611; RRID: AB_321239
Alexa Fluor 647 Goat anti-rat IgG (H+L) (1:200)	Invitrogen	Ref:A21247 Lot:2311802; RRID: AB_141778
Experimental models: Organisms/strains		
Drosophila: *fat2ΔICD: fat2ΔICD-3xGFP FRT80B*	Laboratory of S. Horne-Badovinac[27]	N/A
Drosophila: *fat2N103-2: fat2N103-2 FRT80B*	Laboratory of S. Horne-Badovinac[25]	N/A
Drosophila: *Or47b-GAL4 Or23a-GAL4 Or47a-Gal4 Gr21a-GAL4 UAS-SytGFP*	Laboratory of L. Vosshall[84]	N/A
Drosophila: *UAS-fat2 RNAi (kug)*	Bloomington Drosophila Stock Center	BDSC 40888
Drosophila: *fat2-58D*	Laboratory of C. Dahmann[39]	N/A
Drosophila: *Fat2-3xGFP FRT80B*	Laboratory of S. Horne- Badovinac[27]	N/A
Drosophila: *UAS-mCD8GFP*	Laboratory of P. Volkan	N/A
Drosophila: *eyFLP*	Bloomington Drosophila Stock Center	BDSC 5580
Drosophila: *UAS>STOP>mCD8GFP*	Bloomington Drosophila Stock Center	BDSC 30032
Drosophila: *Fat2-GAL4 (kug)*	Bloomington Drosophila Stock Center	BDSC 77610
Drosophila: *Or19a-GAL4*	Bloomington Drosophila Stock Center	BDSC 24617
Drosophila: *Or69a-GAL4*	Silbering et al.[41]	BDSC 9999
Drosophila: *Ir40a-GAL4*	Silbering et al.[41]	BDSC 41727
Drosophila: *Ir64a-GAL4*	Silbering et al.[41]	BDSC 41732
Drosophila: *Ir84a-GAL4*	Silbering et al.[41]	BDSC 41734
Drosophila: *Or22-GAL4*	Silbering et al.[41]	N/A
Drosophila: *Or88a-mCD8GFP*	Fishilevich and Vosshall[84]	N/A
Drosophila: *72OK-GAL4 UAS-sytGFP*	Laboratory of P. Volkan	N/A
Drosophila: *UAS-sytGFP*	Laboratory of P. Volkan	N/A
Drosophila: *10xUAS-mCD8RFP*	Bloomington Drosophila Stock Center	BDSC 32219
Drosophila: *499-GAL4*	Liou et al.[49]	BDSC 63325
Drosophila: *peb-GAL4; Or47b/Or23a/ Gr21a- SytGFP/CYO;TM2/TM6B*	Laboratory of P. Volkan	N/A

(*Continued on next page*)

Continued

REAGENT or RESOURCE	SOURCE	IDENTIFIER
Drosophila: *UAS-Apc RNAi*	Bloomington Drosophila Stock Center	BDSC 34869
Drosophila: *UAS-CG17528 (zyg8) RNA*	Bloomington Drosophila Stock Center	BDSC 42575
Drosophila: *UAS-Chb RNAi*	Bloomington Drosophila Stock Center	BDSC 35442
Drosophila: *UAS-dop RNA*	Bloomington Drosophila Stock Center	BDSC 60138
Drosophila: *dop1 red1 e1/TM6B, Tb1 (dop1)*	Bloomington Drosophila Stock Center	BDSC 64424
Drosophila: *Apc2N175K ApcQ8/TM3*	Bloomington Drosophila Stock Center	BDSC 7211
Deposited data		
Single-cell RNA-seq data for developing ORNs	McLaughlin et al.[32]	GEO: GSE162121
Customized code for single-cell RNA-seq data analysis and visualization	This paper	https://github.com/volkanlab/Vien_fat2_iScience2024
Software and algorithms		
GraphPad Prism 9	GraphPad	N/A
R 4.3.1	R Core Team	https://www.R-project.org/
FV10-ASW Viewer software 04.02	Olympus confocal system software	N/A
ChatGPT3	OpenAI	https://chatgpt.com/?oai-dm=1
FIJI	https://imagej.net/software/fiji/	N/A
Adobe Illustrator	Adobe	https://www.adobe.com/products/illustrator.html

RESOURCE AVAILABILITY

Lead contact

Further information and requests for resources and reagents should be directed to and will be fulfilled by the lead contact, Pelin Volkan (pelin.volkan@duke.edu).

Materials availability

This study did not generate new unique reagents.

Data and code availability

Data: Single-cell RNA-seq data was previously published[32] and the accession number is listed in the key resources table. All data reported in this paper will be shared by the lead contact upon request.

Code: All original code used to analyze and visualize the single-cell RNA-seq data can be found in https://github.com/volkanlab/Vien_fat2_iScience2024.

Additional information: Any additional information required to reanalyze the data reported in this paper is available from the lead contact upon request.

EXPERIMENTAL MODEL AND STUDY PARTICIPANT DETAILS

Genetics, fly husbandry, and RNAi knockdown

Flies were kept at room temperature or 25 degrees. For RNAi experiments, RNAi crosses were reared at 28°C and only moved to RT (room temperature) on the day of dissection. Flies were dissected 3-7 days after eclosion. To restrict background variation, we collected RNAi knock down only, No-GAL4 control, and genetic interaction flies from the same cross. Males and females are equally included in the sample size where genetically applicable. All experiments conform to the relevant regulatory standards.

ORN specific knockdown of *fat2* RNAi utilized *peb-GAL4; UAS-fat2 RNAi* (BDSC:40888); Or47b-mCD8GFP. LN specific knockdown of *fat2* RNAi utilized *UAS-kug RNAi* (BDSC:40888); Or47b-mCD8GFP/ *449-GAL4* (LN-subtype specific marker, BDSC:63325).

METHOD DETAILS

Immunohistochemistry and image acquisition

Flies were immobilized by and washed in 70% ethanol for 30 seconds and then moved to .1% PBT (Phosphate Buffer Solution with .1% Triton X-100). Brains were removed via micro dissection and immediately placed in .4% PFA (paraformaldehyde) on ice. Then the brains were fixed in 4% PFA for 15 to 30 minutes at room temperature. Then washed in PBT 3x for 20 minutes each wash.

For immunostaining primary antibodies were used at the following concentrations: rabbit α-GFP 1:1000 (Invitrogen), rat α-Ncad 1:20 (Developmental Studies Hybridoma Bank), mouse α-rat CD2 1:200 (Serotec), Secondary antibodies were used at the following concentrations: AlexaFluor488 goat α-rabbit 1:1000, AlexaFluor568 goat α-mouse IgG highly cross-adsorbed 1:300, AlexaFluor647 goat α-rat 1:200. Confocal images taken using an Olympus Fluoview FV1000 at 40x.

Stacks of optical sections 2 μm thick were collected on Olympus Fluoview FV1000 of the entire antennal lobe. Z-stack projections created on either Fluoview or FIJI and then imported into Adobe Illustrator to generate figures.

72OK-GAL4 developmental time point analysis

One batch of brains (about 15 brains per batch) between 18 hAPF and 30 hAPF were dissected, imaged, and then visually assessed for age.[3,4,41] Another batch of brains 24 hAPF to 50 hAPF were dissected, imaged, and then visually assessed for age. Developmental time point was determined using brain morphology found in both groups indicate brains aged between 24 hAPF to 30 hAPF. Fat2 null mutant brains presented with the same proportion of phenotypic developing brains as compared to adult mutant brains (about 35% phenotypic penetrance in developing brains).

QUANTIFICATION AND STATISTICAL ANALYSIS

Phenotypic scoring

For our scoring criteria of brains labeled with a single glomerulus: both antennal lobes are assessed for glomerular disruptions. Each brain is given a score of 0 (wild type) to 4 (severe disruption). Please see Figure S9 for further clarification of phenotypes. Severity is determined by whether the morphology is present in control brains, and if present then at what percentage. Only brains with a score 3 and/or 4 is considered disrupted. 0 score is for brains that nearly identically mirrors the most common glomerular morphology present in our control group. 1 or 2 scores are given to glomerular morphologies that are seen in a small minority (less than 15% of control group brains may have this morphology) of control group brains. The numbers 1 and/or 2 does not indicate an increase in the severity of the phenotype, instead the two scores are available only when multiple categories of minority morphologies are seen in the control group (such as mild positional rearrangement of the glomeruli or mild shape change such as thinning of the glomerulus). Brains marked 1 or 2 are ultimately considered wild-type/control when we calculate phenotypic penetrance. The scores 3 and 4 are given to glomerular morphologies that are rarely (less than 3% of control brains have the phenotype), if ever, seen in the control group. Again, two numbers are provided not to indicate differing severity but to distinguish between categories of morphology such as a drastic positional shift vs. a drastic fragmentation of the glomeruli. Brains with multiple glomeruli labeled are considered disrupted if at least one glomerulus presents with a score 3 or 4 morphology.

Fat2 protein expression analysis and intersectional labeling

Developmental analysis of Fat2 protein expression was obtained using CRISPR generated Fat2-3xGFP flies graciously gifted to us by the Horne-Badovinac Lab.[27] White pupa (staged as 0 hAPF) were collected on a microscope slide, then placed in a closed petri dish with a damp kim wipe for ~24hrs, ~48hrs, and ~72hrs (may vary ±3 hours). Both brains and antenna were dissected, immunostained, and imaged.

To intersectionally label *fat2* expressing cells we used cell type specific FLP/FRT (*ey-FLP* for ORN specific labeling, and *GH146-FLP* for PN specific labeling) in conjunction with *fat2*-GAL4 and *UAS>stop>GFP* system to intersectional label cell type specific expression patterns for *fat2*. Time point collection, dissection, and imaging performed according to immunohistochemistry methods section.

To categorize Or classes based on fluorescence intensity (Figures 2G and 2H), the brains were imaged at three different laser levels (1%, 3%, and 5%) to visualize dim signals (which might oversaturate bright glomeruli) and bright signals (which could miss dimly fluorescent glomeruli). After acquiring images and selecting the most representative laser level/brain, we pseudo-colored the Fat2-3xGFP fluorescence intensity using the "Thermal" LUT in the Olympus Fluoview software. The "Thermal" LUT, also known as "Spec3", assigns the pixel with the highest intensity throughout the z-projection as 4095 and sets the lowest intensity pixel as 0. It then bins pixel intensity values into three groups and assigns an intensity value to a corresponding color, with red representing the highest intensity value and black/dark blue representing the lowest intensity value (background outside the brain). High-expressing glomeruli are categorized as those containing pixels with intensity levels within the highest one third of the entire intensity dynamic range, visually represented as yellow to red coloration. We observed that some glomeruli do not maintain the same intensity level throughout, so we decided to categorize based on the highest pixel intensity present anywhere within each glomerulus. Note that white coloration indicates pixels that have reached the maximum intensity and are likely oversaturated. Low-expressing glomeruli are categorized as those containing pixels with intensity levels corresponding to the lowest third of the full intensity range, which corresponds to black to light blue coloration.

To quantify fluorescence intensity, we loaded the entire confocal files capturing each brain into FIJI (Fiji is just imagej). Then using the Ncad channel to locate the specified glomerulus. Or-class selection was based on Or classes with the most stereotyped glomeruli morphology that was also relatively stable and developed by 50 hAPF. We made a concerted effort to include Or classes in high, medium, and low Fat2

expressing categories. Once located, we use the free draw tool to outline the glomerulus. Then we identified how many z-slices the glomerulus spanned and switch to the GFP channel to measure the average fluorescence intensity (within the ROI we've drawn) across the appropriate z-slices. This process is then repeated for the other antennal lobe. Background fluorescence was established using a square ROI directly dorsal of the antennal lobe, but outside of the antennal lobe, approximately equal to one-fifth of the area of the entire antennal lobe. Background was also collected across z slices and from both hemispheres of the brain.

We used PRISM9 to create the aligned scatter plot in Figure S2. Each data point is one measurement, each Or class contains fluorescence measurements across z-slices as well as from both antennal lobes.

Statistics

As for statistics, P-value was calculated by two-tailed Fisher's exact test through the built-in functions of GraphPad Prism 9 software. All n numbers represent biological replicates, each n is an individual fly.

Analyzing the *fat2* expression in the single-cell RNA-seq datasets

The annotated single-cell RNA-seq datasets were from McLaughlin et al.[32] (GSE162121). We extracted the expression values ($\log_2$(CPM +1)) of *fat2* (*kug*) across all the cells assigned to ORN classes. We calculated the fraction of *fat2*-positive cells (defined by $\log_2$(CPM +1) $\geq$ 1) and the mean expression of *fat2* of each ORN class at each developmental stage.